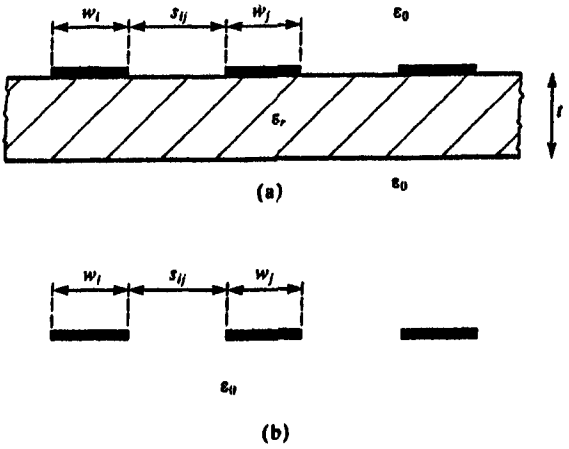

FIGURE 3.32 A printed circuit board (PCB) for illustration of the determination of the per-unit-length capacitances.

edge-to-edge separations are denoted as s_{ij}. A direct approach would be to subsection each land into N_i segments of length w_{ik}. The charge on each subsection could be represented using the pulse expansion method as being constant over that segment with unknown level of α_{ik}. We could similarly subsection the surface of the dielectric and represent the bound charge on that surface with pulse expansions. A more direct way would be to imbed the dielectric in the basic *Green's function.* We will choose to do this. Thus the problem becomes one of subsectioning the conductors immersed in free space as illustrated in Fig. 3.32(b).

First we consider solving the problem with the board removed as in Fig. 3.32(b) then we will consider adding the board. Consider the subproblem of a strip of width w representing one of the subsections of a land shown in Fig. 3.33(a). We need to find the potential at a point a distance d from the strip center and in the plane of the strip. This basic subproblem was solved earlier and the results of (3.105) and (3.107) specialized to this case are

$$\phi_{self}(w) = \frac{1}{2\pi\varepsilon_o}\left[w - w\ln\left(\frac{w}{2}\right)\right] \tag{3.114a}$$

$$= \frac{w}{2\pi\varepsilon_o}\left[1 - \ln\left(\frac{w}{2}\right)\right]$$

$$\phi(w,d) = \frac{1}{2\pi\varepsilon_o}\left[w + \left(d - \frac{w}{2}\right)\ln\left(d - \frac{w}{2}\right) - \left(d + \frac{w}{2}\right)\ln\left(d + \frac{w}{2}\right)\right] \tag{3.114b}$$

$$= \phi_{self}(w) + \frac{w}{2\pi\varepsilon_o}\left[\tfrac{1}{2}(2D-1)\ln(2D-1) - \tfrac{1}{2}(2D+1)\ln(2D+1)\right]$$

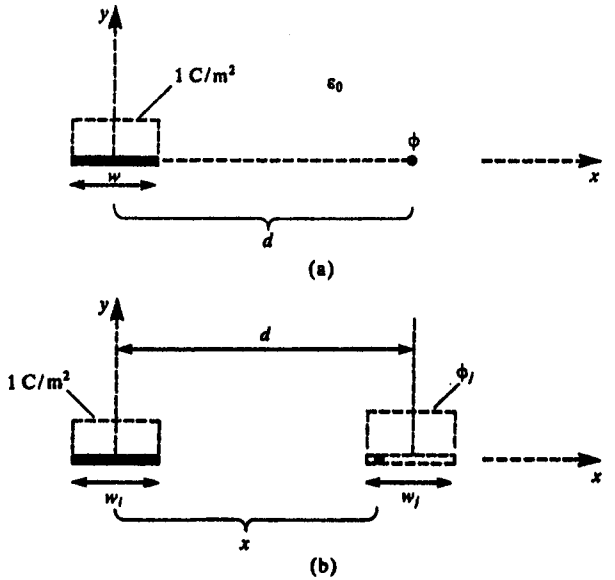

FIGURE 3.33 Illustration of the determination of the potential due to a constant charge distribution on a flat strip via (a) point matching and (b) the Galerkin method.

The mutual result in (3.114b) is written in terms of the self term in (3.114a) and the ratio of the separation to subsection width:

$$D = \frac{d}{w} \tag{3.114c}$$

It is interesting to note that for the case of pulse expansions, the total per-unit-length charge on a strip is simply the strip width, i.e.,

$$q = (1\ \text{C/m}^2) \times w = w$$

Thus if only one subdivision is used per land, the terms in (3.114a) and (3.114b) are the entries in the *inverse* of the generalized capacitance matrix. In the case that the lands are divided into more than one subsection, these terms represent the entries in the inverse of a *global generalized capacitance matrix* as though each land consisted of several unconnected sublands.

The Galerkin method given by (3.111) obtains these basic subproblems as illustrated in Fig. 3.33(b) and uses (3.114b):

$$w_j \phi_j(w_j, d) = \int_{d-w_j/2}^{d+w_j/2} 1 \phi_j(w_i, x)\, dx \tag{3.115}$$

continued

$$= \frac{1}{2\pi\varepsilon_o} \int_{d-w_j/2}^{d+w_j/2} 1\left[w_i + \left(x - \frac{w_i}{2}\right)\ln\left(x - \frac{w_i}{2}\right) - \left(x + \frac{w_i}{2}\right)\ln\left(x + \frac{w_i}{2}\right)\right] dx$$

or [8]

$$w_i \phi_{i,\text{self}}(w_i) = \frac{1}{2\pi\varepsilon_o}\left[\tfrac{3}{2} w_i^2 - w_i^2 \ln(w_i)\right] \tag{3.116a}$$

$$= \frac{w_i^2}{2\pi\varepsilon_o}\left[\tfrac{3}{2} - \ln(w_i)\right]$$

for the self terms and

$$\begin{aligned} w_j \phi_j(w_i, d) = \frac{1}{2\pi\varepsilon_o} \Bigg\{ & w_i w_j - \frac{1}{2}\left[d + \frac{(w_j - w_i)}{2}\right]^2 \left[\frac{1}{2} - \ln\left(d + \frac{(w_j - w_i)}{2}\right)\right] \\ & + \frac{1}{2}\left[d - \frac{(w_j + w_i)}{2}\right]^2 \left[\frac{1}{2} - \ln\left(d - \frac{(w_j + w_i)}{2}\right)\right] \\ & + \frac{1}{2}\left[d + \frac{(w_j + w_i)}{2}\right]^2 \left[\frac{1}{2} - \ln\left(d + \frac{(w_j + w_i)}{2}\right)\right] \\ & - \frac{1}{2}\left[d - \frac{(w_j - w_i)}{2}\right]^2 \left[\frac{1}{2} - \ln\left(d - \frac{(w_j - w_i)}{2}\right)\right]\Bigg\} \\ = \frac{1}{2\pi\varepsilon_o} \Bigg\{ & \frac{3}{2} w_i w_j + \frac{1}{2}\left[d + \frac{(w_j - w_i)}{2}\right]^2 \ln\left(d + \frac{(w_j - w_i)}{2}\right) \\ & - \frac{1}{2}\left[d - \frac{(w_j + w_i)}{2}\right]^2 \ln\left(d - \frac{(w_j + w_i)}{2}\right) \\ & - \frac{1}{2}\left[d + \frac{(w_j + w_i)}{2}\right]^2 \ln\left(d + \frac{(w_j + w_i)}{2}\right) \\ & + \frac{1}{2}\left[d - \frac{(w_j - w_i)}{2}\right]^2 \ln\left(d - \frac{(w_j - w_i)}{2}\right)\Bigg\} \end{aligned} \tag{3.116b}$$

for the mutual terms. If we specialize this to strips of equal width, $w_i = w_j = w$, these results simplify to

$$w\phi_{\text{self}}(w) = \frac{1}{2\pi\varepsilon_o}\left[\tfrac{3}{2} w^2 - w^2 \ln(w)\right] \tag{3.117a}$$

$$w\phi(w, d) = \frac{1}{2\pi\varepsilon_o}\left[\tfrac{3}{2} w^2 + d^2 \ln(d) - \tfrac{1}{2}(d - w)^2 \ln(d - w) - \tfrac{1}{2}(d + w)^2 \ln(d + w)\right] \tag{3.117b}$$

Dividing both sides by the common subsection width, w, these results can again be written in terms of the self term and the ratio of the subsection separation

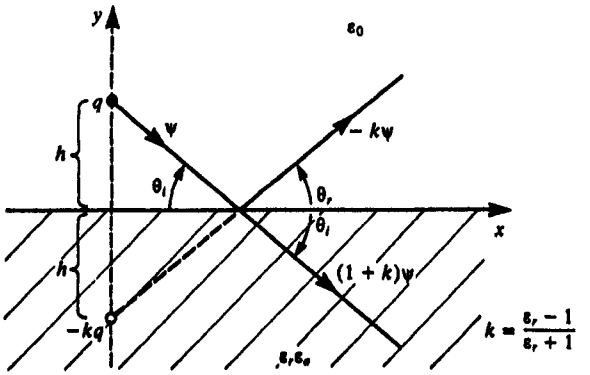

FIGURE 3.34 Illustration of the method of images for a point charge above an infinite dielectric half-space.

to width ratio, D, given in (3.114c) as

$$\phi_{self}(w) = \frac{w}{2\pi\varepsilon_o}\left[\tfrac{3}{2} - \ln(w)\right] \tag{3.117c}$$

$$\phi(w, d) = \phi_{self}(w) + \frac{w}{2\pi\varepsilon_o}\left[D^2 \ln(D) - \tfrac{1}{2}(D-1)^2 \ln(D-1)\right. \tag{3.117d}$$
$$\left. - \tfrac{1}{2}(D+1)^2 \ln(D+1)\right]$$

Next consider incorporating the dielectric board into these basic results. The first problem that needs to be solved is that of an infinite (in the z direction) line charge of q C/m situated a height h above the plane interface between two dielectric media as shown in Fig. 3.34. The upper half-space has free space permittivity ε_o and the lower half-space has permittivity $\varepsilon = \varepsilon_r\varepsilon_o$. This classic problem allows one to compute the potential in each region by images in the same fashion as though the lower region were a perfect conductor [3, 10]. The solution can be obtained by visualizing lines or tubes of electric flux, ψ, from the line charge. Electric flux lines through some open surface s are related to the electric flux density vector, $\vec{\mathscr{D}} = \varepsilon\vec{\mathscr{E}}$, as $\psi = \iint_s \vec{\mathscr{D}} \cdot d\vec{s}$. Consider one such flux line emanating from the line charge which is incident on the interface at some angle θ_i. Some of this flux passes through the interface as $(1 + k)\psi$ while some is reflected at an angle θ_r as $-k\psi$. Snell's law shows that $\theta_i = \theta_r$. The boundary conditions at the interface require that the normal components of the electric flux density be continuous, i.e.,

$$\psi \sin\theta_i + k\psi \sin\theta_r = (1 + k)\psi \sin\theta_i \tag{3.118a}$$

Similarly, the tangential components of the electric field must be continuous

across the interface giving

$$\frac{1}{\varepsilon_o}\psi \cos\theta_i - \frac{1}{\varepsilon_o}k\psi \cos\theta_r = \frac{1}{\varepsilon_r\varepsilon_o}(1+k)\psi \cos\theta_i \tag{3.118b}$$

Recalling that $\theta_i = \theta_r$ gives

$$k = \frac{\varepsilon_r - 1}{\varepsilon_r + 1} \tag{3.119a}$$

and

$$\alpha = (1+k) = \frac{2\varepsilon_r}{\varepsilon_r + 1} \tag{3.119b}$$

and (as will be needed later)

$$(1-k^2) = \frac{\alpha^2}{\varepsilon_r} \tag{3.119c}$$

Thus the potential in the upper half-space ($y > 0$) is as though it were due to the original charge, q, at the original height h and an image charge, $-kq$, with the dielectric removed and at a distance h below the interface:

$$\phi^+(x,y) = -\frac{q}{4\pi\varepsilon_o}\ln[x^2 + (y-h)^2] + \frac{kq}{4\pi\varepsilon_o}\ln[x^2 + (y+h)^2] \tag{3.120a}$$

The potential below the interface ($y > 0$) is due to a line charge $(1+k)q$ located a height h above the interface with the upper free-space region replaced by the dielectric:

$$\phi^-(x,y) = -\frac{\alpha q}{4\pi\varepsilon_r\varepsilon_o}\ln[x^2 + (y-h)^2] \tag{3.120b}$$

The problem now of interest is a line charge on the surface of a dielectric slab (the PCB) of relative permittivity ε_r and thickness t. First consider the more general problem of a line charge q located a height h above the dielectric slab. Using the above results we may construct the diagram of Fig. 3.35. These results follow similar lines as in optics. Observe that the potential in each of the three regions appear due to line charge images that produce the solid flux tubes in that region, and the appropriate dielectric constant to be used in the potential expression is that of the region. Now consider the problem at hand of a line charge on the surface of a dielectric slab of relative permittivity ε_r and thickness t as shown in Fig. 3.36(a). We wish to find the potential at a point on the board a distance d from the line charge. Specializing the results of Fig. 3.35 for $h = 0$ gives the images shown in Fig. 3.36(b). The potential then takes the form of a

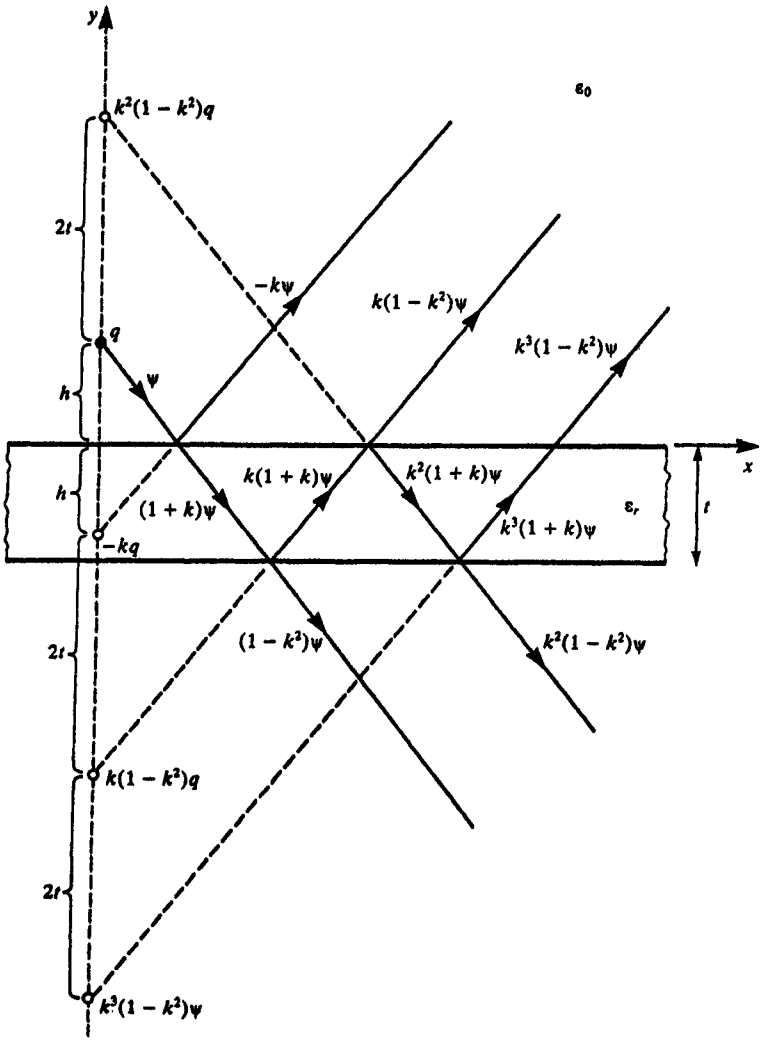

FIGURE 3.35 Images of a point charge above a dielectric slab of finite thickness.

series:

$$\phi(d) = -\frac{\alpha q}{4\pi\varepsilon_r\varepsilon_o}\ln(d^2) - \frac{\alpha^2 q}{4\pi\varepsilon_r\varepsilon_o}\sum_{n=1}^{\infty} k^{(2n-1)}\ln[d^2 + (2nt)^2] \qquad (3.121)$$

This series converges rapidly since $k < 1$.

Applying this result for a line charge to an infinitesimally thin strip on a dielectric slab by representing the charge distribution (pulse expansion function) as a set of 1 C/m line charges as shown in Fig. 3.37(a) requires performing the

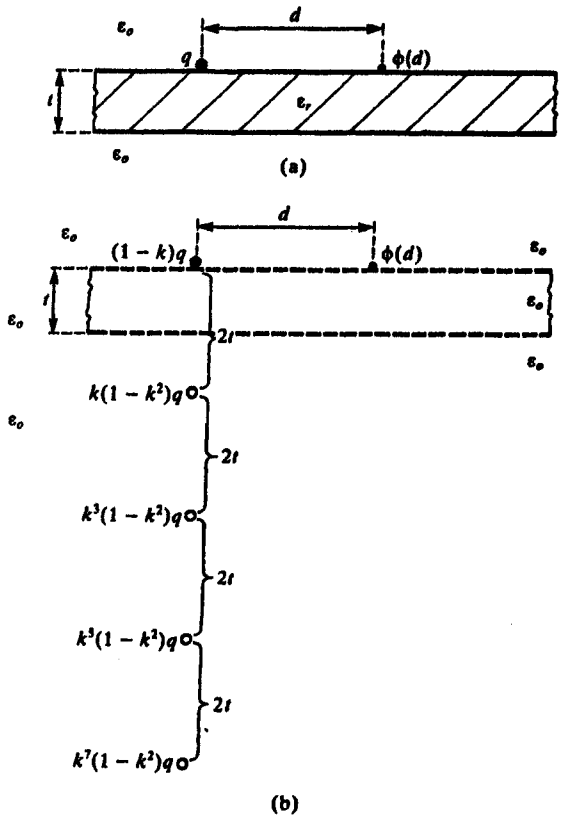

FIGURE 3.36 Illustration of the replacement of a dielectric slab of finite thickness with images to be used in modeling a PCB.

following integral:

$$\phi(d) = -\frac{\alpha}{4\pi\varepsilon_r\varepsilon_o}\int_{-w/2}^{w/2} \ln[(x+d)^2]\,dx \qquad (3.122)$$
$$-\frac{\alpha^2}{4\pi\varepsilon_r\varepsilon_o}\sum_{n=1}^{\infty} k^{(2n-1)}\int_{-w/2}^{w/2} \ln[(x+d)^2+(2nt)^2]\,dx$$

The result is

$$\phi_{\text{self}}(w) = \frac{1}{2\pi\varepsilon_o}\frac{\alpha}{\varepsilon_r}\left[w - w\ln\left(\frac{w}{2}\right)\right] + \frac{1}{2\pi\varepsilon_o}\frac{\alpha^2}{\varepsilon_r}\sum_{n=1}^{\infty} k^{(2n-1)} \qquad (3.123a)$$
$$\times\left\{w - \frac{w}{2}\ln\left[\left(\frac{w}{2}\right)^2 + a^2\right] - 2a\tan^{-1}\left(\frac{w}{2a}\right)\right\}$$

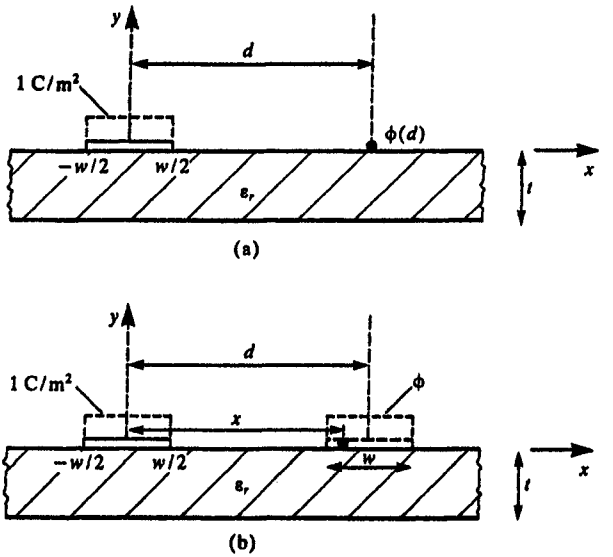

FIGURE 3.37 Illustration of the determination of the per-unit-length capacitances for a PCB by (a) point matching and (b) the Galerkin method.

and

$$\phi(w,d) = \frac{1}{2\pi\varepsilon_o}\frac{\alpha}{\varepsilon_r}\left[w + \left(d-\frac{w}{2}\right)\ln\left(d-\frac{w}{2}\right) - \left(d+\frac{w}{2}\right)\ln\left(d+\frac{w}{2}\right)\right] \tag{3.123b}$$

$$+ \frac{1}{2\pi\varepsilon_o}\frac{\alpha^2}{\varepsilon_r}\sum_{n=1}^{\infty} k^{(2n-1)}$$

$$\times\left\{w + \frac{1}{2}\left(d-\frac{w}{2}\right)\ln\left[\left(d-\frac{w}{2}\right)^2 + a^2\right] - \frac{1}{2}\left(d+\frac{w}{2}\right)\right.$$

$$\left.\times\ln\left[\left(d+\frac{w}{2}\right)^2 + a^2\right] + a\left[\tan^{-1}\left(\frac{d-\frac{w}{2}}{a}\right) - \tan^{-1}\left(\frac{d+\frac{w}{2}}{a}\right)\right]\right\}$$

where $a = 2nt$. These results can be simplified and written in terms of the potentials with the dielectric removed as

$$\phi_{\text{self}}(w) = \phi^{o}_{\text{self}}(w) - \frac{w}{2\pi\varepsilon_o\varepsilon_r'}\alpha\sum_{n=1}^{\infty} k^{(2n-1)} \tag{3.123c}$$

$$\times\left\{\frac{1}{2}\ln[1 + (4nT)^2] + 4nT\tan^{-1}\left(\frac{1}{4nT}\right)\right\}$$

and

$$\phi(w,d) = \phi^o(w,d) + \frac{w}{2\pi\varepsilon_o\varepsilon_r'} \alpha \sum_{n=1}^{\infty} k^{(2n-1)} \tag{3.123d}$$
$$\times \left\{ -\tfrac{1}{2}(2D-1)\ln(2D-1) + \tfrac{1}{2}(2D+1)\ln(2D+1) + \tfrac{1}{4}(2D-1) \right.$$
$$\times \ln[(2D-1)^2 + (4nT)^2] - \tfrac{1}{4}(2D+1)\ln[(2D+1)^2 + (4nT)^2]$$
$$\left. + \frac{1}{2}(4nT)\left[\tan^{-1}\left(\frac{2D-1}{4nT}\right) - \tan^{-1}\left(\frac{2D+1}{4nT}\right)\right]\right\}$$

where $\phi^o_{self}(w)$ is the self term with the dielectric removed given in (3.114a), and $\phi^o(w,d)$ is the mutual term with the dielectric removed given in (3.114b). The results have been written in terms of the ratios of subsection to subsection width, D, and board thickness to land width, T:

$$D = \frac{d}{w} \tag{3.123e}$$

and

$$T = \frac{t}{w} \tag{3.123f}$$

Additionally the notation

$$\varepsilon_r' = \frac{(\varepsilon_r + 1)}{2} \tag{3.123g}$$

denotes the effective dielectric constant as the board thickness becomes infinite, $t \to \infty$, such that it fills the lower half-space. This notion of an effective dielectric constant for this case is valid since half the electric field lines would exist in air and the other in the infinite half-space occupied by the board. Evidently the summation terms in (3.123c) and (3.123d) give the effect of the board. These results are used in the FORTRAN program **PCB.FOR** described in Appendix A to compute the entries in the per-unit-length capacitance matrix **C** of a PCB. The per-unit-length inductance matrix **L** is computed with the board removed from the basic relationship derived earlier:

$$\mathbf{L} = \mu_o\varepsilon_o\mathbf{C}_o^{-1} \tag{3.124}$$

where $\mathbf{C}_o$ is the per-unit-length capacitance matrix with the board removed.

The Galerkin solution (specialized to equal width strips) is similarly obtained

from Fig. 3.37(b), (3.111), and (3.123b) as the basic integral

$$w\phi(w,d) = \frac{1}{2\pi\varepsilon_o}\frac{\alpha}{\varepsilon_r} \tag{3.125}$$
$$\times \int_{d-w/2}^{d+w/2r} \left[w + \left(x - \frac{w}{2}\right)\ln\left(x - \frac{w}{2}\right) - \left(x + \frac{w}{2}\right)\ln\left(x + \frac{w}{2}\right)\right] dx$$
$$+ \frac{1}{2\pi\varepsilon_o}\frac{\alpha^2}{\varepsilon_r}\sum_{n=1}^{\infty} k^{(2n-1)}$$
$$\times \int_{d-w/2}^{d+w/2} \left\{ w + \frac{1}{2}\left(x - \frac{w}{2}\right)\ln\left[\left(x - \frac{w}{2}\right)^2 + a^2\right] - \frac{1}{2}\left(x + \frac{w}{2}\right)\right.$$
$$\times \ln\left[\left(x + \frac{w}{2}\right)^2 + a^2\right]$$
$$\left. + a\left[\tan^{-1}\left(\frac{x - \frac{w}{2}}{a}\right) - \tan^{-1}\left(\frac{x + \frac{w}{2}}{a}\right)\right]\right\}$$

The result is

$$w\phi_{self}(w) = \frac{w^2}{2\pi\varepsilon_o}\frac{\alpha}{\varepsilon_r}\left[\tfrac{3}{2} - \ln(w)\right] + \frac{w^2}{2\pi\varepsilon_o}\frac{\alpha^2}{\varepsilon_r}\sum_{n=1}^{\infty} k^{(2n-1)} \tag{3.126a}$$
$$\times \left\{\frac{3}{2} - \ln(a) + \frac{1}{2}\left[\left(\frac{a}{w}\right)^2 - 1\right]\ln\left[\left(\frac{w}{a}\right)^2 + 1\right] - \frac{2a}{w}\tan^{-1}\left(\frac{w}{a}\right)\right\}$$

and

$$w\phi(w,d) = \frac{w^2}{2\pi\varepsilon_o}\frac{\alpha}{\varepsilon_r}\left[\frac{3}{2} - \ln(w) + \left(\frac{d}{w}\right)^2\ln\left(\frac{d}{w}\right)\right. \tag{3.126b}$$
$$\left. - \frac{1}{2}\left(\frac{d}{w} - 1\right)^2\ln\left(\frac{d}{w} - 1\right) - \frac{1}{2}\left(\frac{d}{w} + 1\right)^2\ln\left(\frac{d}{w} + 1\right)\right]$$
$$+ \frac{w^2}{2\pi\varepsilon_o}\frac{\alpha^2}{\varepsilon_r}\sum_{n=1}^{\infty} k^{(2n-1)}$$
$$\times \left\{\frac{3}{2} - \ln(a) + \frac{1}{2}\left[\left(\frac{d}{w}\right)^2 - \left(\frac{a}{w}\right)^2\right]\ln\left[\left(\frac{d}{a}\right)^2 + 1\right]\right.$$
$$- \frac{1}{4}\left[\left(\frac{d}{w} - 1\right)^2 - \left(\frac{a}{w}\right)^2\right]\ln\left[\left(\frac{d/w - 1}{a/w}\right)^2 + 1\right]$$
$$\left. - \frac{1}{4}\left[\left(\frac{d}{w} + 1\right)^2 - \left(\frac{a}{w}\right)^2\right]\ln\left[\left(\frac{d/w + 1}{a/w}\right)^2 + 1\right]\right.$$

continued

$$+\frac{a}{w}\left[2\frac{d}{w}\tan^{-1}\left(\frac{d}{a}\right)-\left(\frac{d}{w}-1\right)\tan^{-1}\left(\frac{d/w-1}{a/w}\right)\right.$$
$$\left.-\left(\frac{d}{w}+1\right)\tan^{-1}\left(\frac{d/w+1}{a/w}\right)\right]\Bigg\}$$

where, again, $a = 2nt$. Dividing the above by the common subsection width, w, these results can again be written in terms of the potential with the board removed and the ratios of separation to width, D, given in (3.123e) and board thickness to width, T, given in (3.123f) as

$$\phi_{self}(w) = \phi^{o}_{self}(w) + \frac{w}{2\pi\varepsilon_o\varepsilon_r'}\alpha\sum_{n=1}^{\infty}k^{(2n-1)} \tag{3.126c}$$
$$\times\left\{\frac{1}{2}[(2nT)^2-1]\ln\left[1+\frac{1}{(2nT)^2}\right]\right.$$
$$\left.-\ln(2nT)-2(2nT)\tan^{-1}\left(\frac{1}{2nT}\right)\right\}$$

and

$$\phi(w,d) = \phi^{o}(w,d) + \frac{w}{2\pi\varepsilon_o\varepsilon_r'}\alpha\sum_{n=1}^{\infty}k^{(2n-1)} \tag{3.126d}$$
$$\times\left\{-D^2\ln(D)+\tfrac{1}{2}(D-1)^2\ln(D-1)\right.$$
$$+\tfrac{1}{2}(D+1)^2\ln(D+1)+\tfrac{1}{2}[D^2-(2nT)^2]\ln[D^2+(2nT)]$$
$$-\tfrac{1}{2}[(D-1)^2-(2nT)^2]\ln[(D-1)^2+(2nT)^2]$$
$$-\tfrac{1}{2}[(D+1)^2-(2nT)^2]\ln[(D+1)^2+(2nT)^2]$$
$$+(2nT)\left[2D\tan^{-1}\left(\frac{D}{2nT}\right)-(D-1)\tan^{-1}\left(\frac{D-1}{2nT}\right)\right.$$
$$\left.\left.-(D+1)\tan^{-1}\left(\frac{D+1}{2nT}\right)\right]\right\}$$

where $\phi^{o}_{self}(w)$ is the self term with the board removed given in (3.117c) and $\phi^{o}(w,d)$ is the mutual term with the board removed given by (3.117d). These results are used to compute the capacitances of PCB's in the FORTRAN program **PCBGAL.FOR** described in Appendix A.

*3.3.1.2 **Computed Results: Printed Circuit Boards*** As an example consider the three-conductor PCB shown in Fig. 3.38 consisting of three conductors of equal width w and identical edge-to-edge separations s. The following computed results are obtained with the FORTRAN programs **PCB.FOR** (pulse expansion

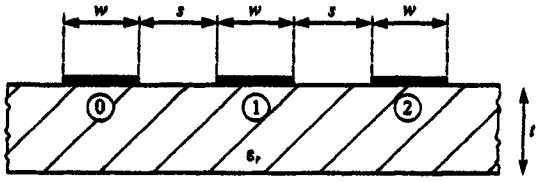

FIGURE 3.38 A PCB consisting of identical conductors with identical separations for computation of numerical results.

functions and point matching) and **PCBGAL.FOR** (pulse expansion functions and Galerkin). The results will be computed for typical board parameters: $\varepsilon_r = 4.7$ (glass epoxy), $t = 47$ mils, $w = s = 15$ mils. Choosing the leftmost conductor as the reference conductor, Fig. 3.39(a) compares the elements of the per-unit-length transmission-line-inductance matrix, **L**, and Fig. 3.39(b) compares the elements of the per-unit-length transmission-line-capacitance matrix, **C**, for the two methods for various numbers of land subdivisions. The Galerkin method converges rather fast and much faster initially than point matching. Figure 3.40 compares the entries in **C** and $\mathbf{C}_0$ for various numbers of land subdivisions. Figure 3.41(a) shows the ratios of the entries in **C** and $\mathbf{C}_0$ for various board thickness using 50 divisions per land computed using the Galerkin method. Observe that these approach an effective dielectric constant that is the average of that of the board and free space:

$$\varepsilon_r' = \frac{\varepsilon_r + 1}{2} = 2.85$$

This would be the effective dielectric constant if the board occupied the infinite half-space since half the electric field lines would reside in free space and the other half in the board. Figure 3.41(b) shows these ratios as a function of the ratio of separation to land width using the Galerkin method and 50 divisions per land. Here we see that for wider separations, the effective dielectric constants are substantially lower than the average assuming the board was infinitely thick. For wide separations, more of the electric field lines exit the bottom of the board and are more important than for closely spaced lands. One might be tempted to obtain *wide-separation approximations* by approximating the charge as being uniformly distributed over each land, which essentially means using pulse expansions and only one division per land. Figure 3.42 shows the results for the inductances and capacitances versus the ratio of separation to land width. These inductances and capacitances give results that are within 10% for $d/w > 5$. However, as we have seen in Fig. 3.41(b), the finite thickness of the dielectric board has more of an effect in the case of wide separations so that an effective dielectric constant is not so easy to obtain.

And finally we will compute the entries in **C** and **L** for a PCB that will be used in later crosstalk analyses: $\varepsilon_r = 4.7$ (glass epoxy), $t = 47$ mils, $w = 15$ mils, and $s = 45$ mils. This separation is such that exactly three lands could be placed

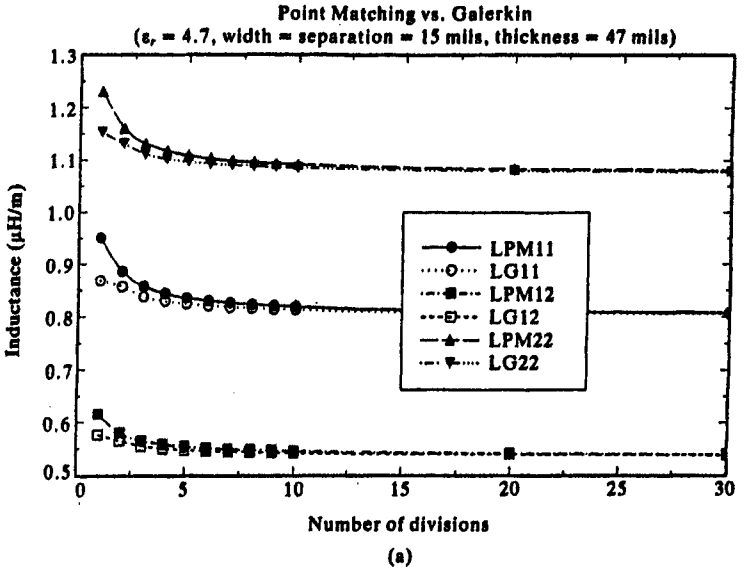

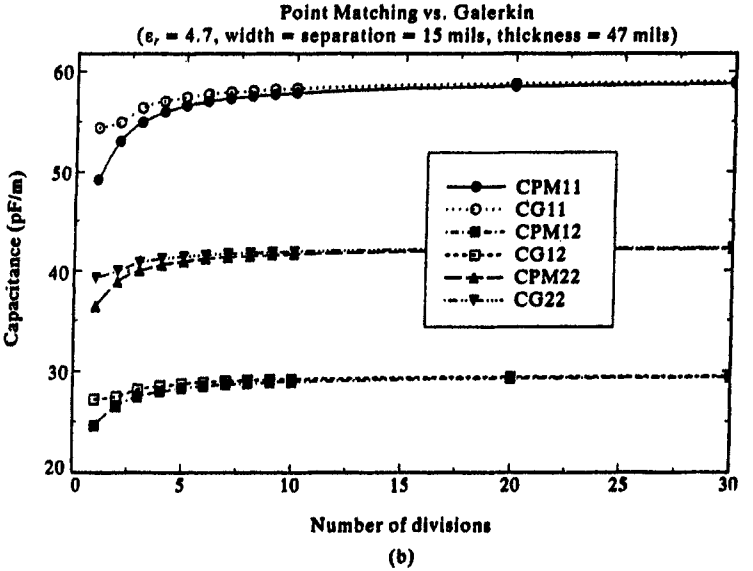

FIGURE 3.39 Illustration of the per-unit-length (a) inductances and (b) capacitances via point matching and via the Galerkin method for various numbers of divisions of each land. $\varepsilon_r = 4.7$, width = separation = 15 mils, thickness = 47 mils.

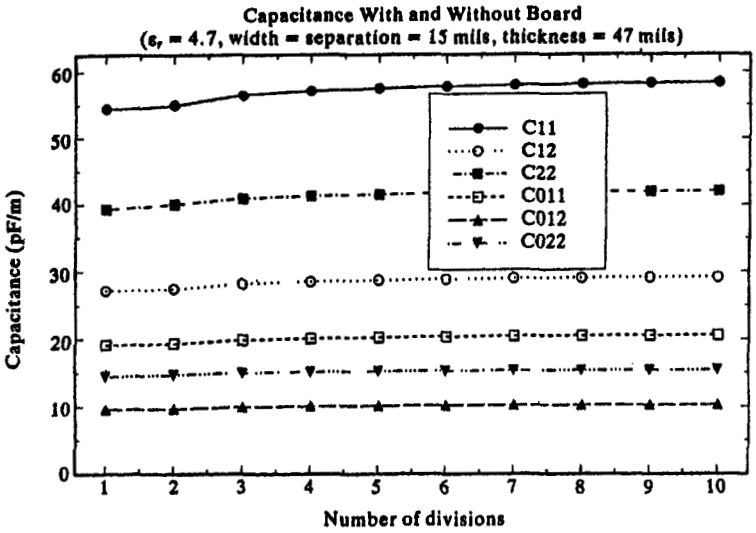

FIGURE 3.40 The capacitances with and without the dielectric board versus the number of divisions per land. $\varepsilon_r = 4.7$, width = separation = 15 mils, thickness = 47 mils.

between any two adjacent lands. The results for the pulse expansion–point matching method for 50 divisions per land are **(PCB.FOR)**

$$\mathbf{L} = \begin{bmatrix} 1.105\,13 & 0.690\,602 \\ 0.690\,602 & 1.381\,20 \end{bmatrix} \mu\text{H/m}$$

$$\mathbf{C} = \begin{bmatrix} 40.599\,1 & -20.299\,6 \\ -20.299\,6 & 29.738\,0 \end{bmatrix} \text{pF/m}$$

The results for the pulse expansion–Galerkin method for 50 divisions per land are **(PCBGAL.FOR)**

$$\mathbf{L} = \begin{bmatrix} 1.104\,18 & 0.690\,094 \\ 0.690\,094 & 1.380\,19 \end{bmatrix} \mu\text{H/m}$$

$$\mathbf{C} = \begin{bmatrix} 40.628\,0 & -20.314\,0 \\ -20.314\,0 & 29.763\,2 \end{bmatrix} \text{pF/m}$$

These compare with the results of a three-dimensional program for finite-width lands of length 10 inches (25.4 cm) and dividing those results by the length of the lands [A.3]:

$$\mathbf{L} = \begin{bmatrix} 1.034\,0 & 0.653\,35 \\ 0.653\,35 & 1.306\,7 \end{bmatrix} \mu\text{H/M}$$

$$\mathbf{C} = \begin{bmatrix} 41.765\,5 & -20.882\,7 \\ -20.882\,7 & 30.502\,2 \end{bmatrix} \text{pF/m}$$

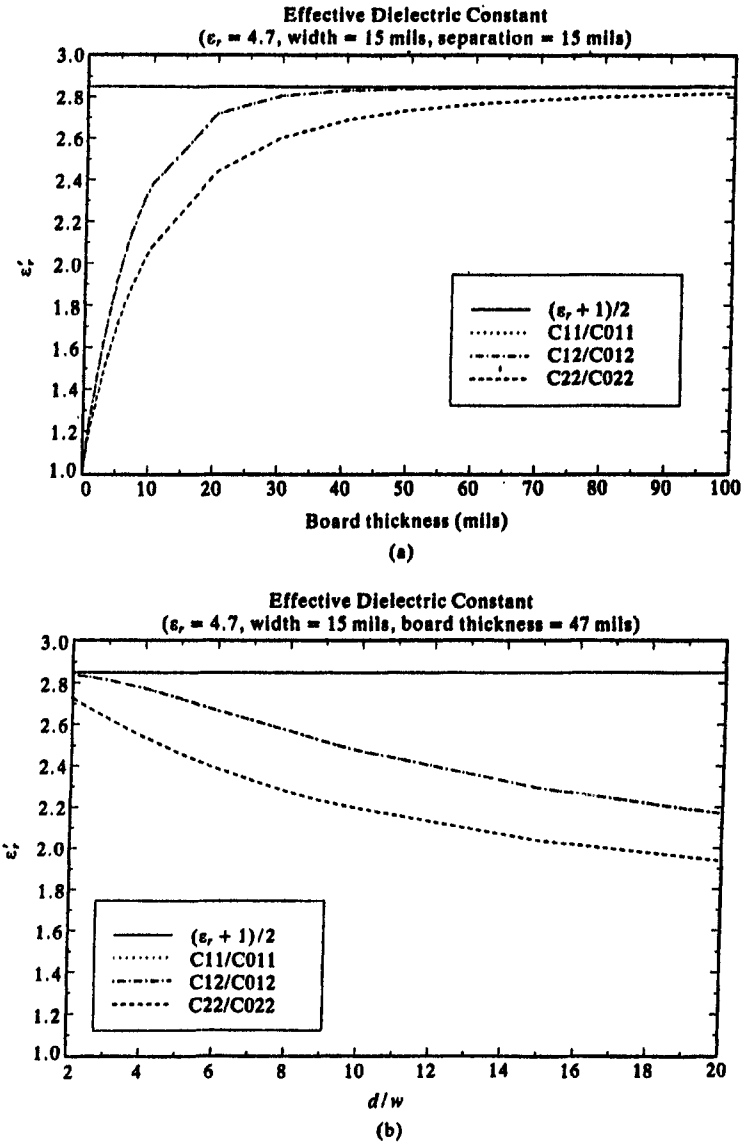

FIGURE 3.41 Illustration of the effective dielectric constant of the PCB versus (a) board thickness (ε_r = 4.7, width = 15 mils, separation = 15 mils); and (b) the ratio of land separation to width ratio (ε_r = 4.7, width = 15 mils, board thickness = 47 mils).

This illustrates that the computations for infinite-length lands (two-dimensional) give adequate results for the per-unit-length parameters for finite-length lands if the lands are much longer than the widths and separations, i.e., the fringing of the electric field at the ends of the lands has negligible effect.

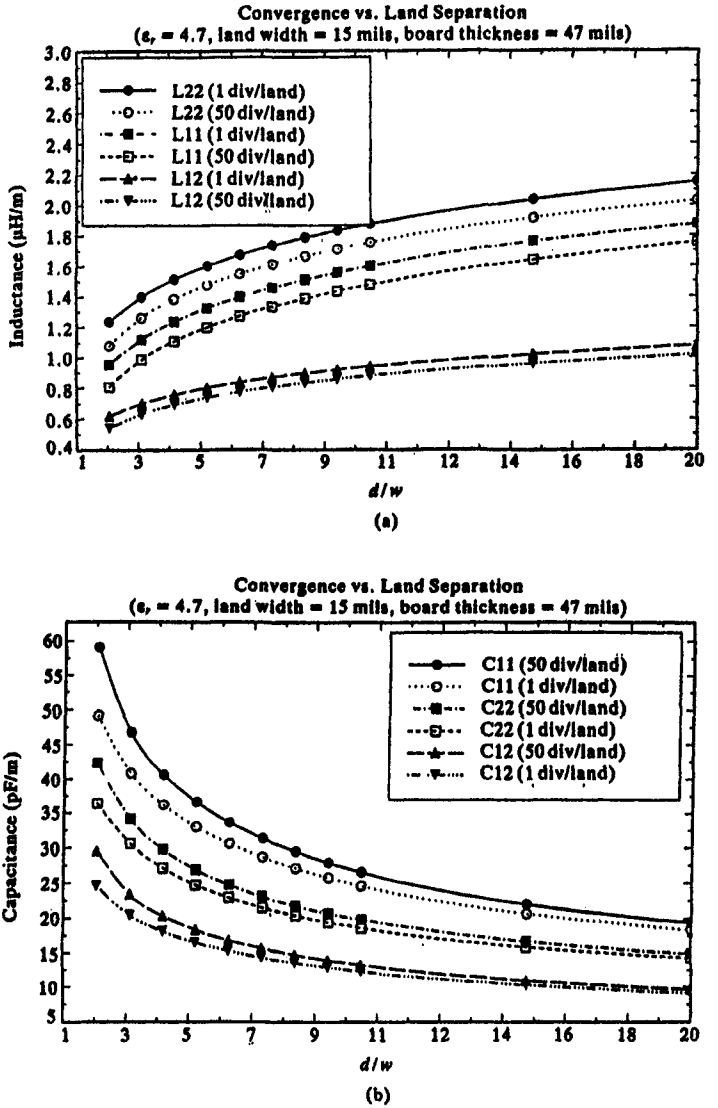

FIGURE 3.42 Illustration of the convergence of (a) inductance and (b) capacitance versus the ratio of land separation to width. $\varepsilon_r = 4.7$, land width = 15 mils, board thickness = 47 mils.

3.3.2 Finite Difference Techniques

Recall that the entries in the per-unit-length inductance, capacitance and conductance matrices are determined as a static (dc) solution for the fields in the transverse (x–y) plane. Essentially, the transverse fields are such that the potential in the space surrounding the conductors, $\phi(x, y)$, again satisfies

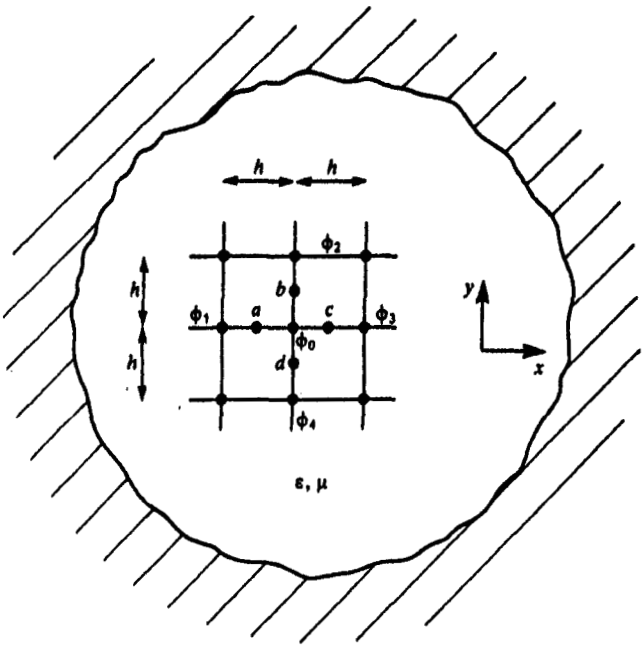

FIGURE 3.43 The finite-difference grid.

Laplace's equation in the transverse plane:

$$\nabla^2\phi(x, y) = \frac{\partial^2\phi(x, y)}{\partial x^2} + \frac{\partial^2\phi(x, y)}{\partial y^2} = 0 \tag{3.127}$$

Finite difference techniques approximate these spatial partial derivatives in a discrete fashion in the space surrounding the conductors. For example, consider the closed region shown in Fig. 3.43. The space is gridded into cells of length and width h. First-order approximations to the first partial derivatives at the interior cell points a, b, c, d are [A.1, 6]

$$\left.\frac{\partial\phi}{\partial x}\right|_a = \frac{\phi_0 - \phi_1}{h} \tag{3.128a}$$

$$\left.\frac{\partial\phi}{\partial x}\right|_c = \frac{\phi_3 - \phi_0}{h} \tag{3.128b}$$

$$\left.\frac{\partial\phi}{\partial y}\right|_b = \frac{\phi_2 - \phi_0}{h} \tag{3.128c}$$

$$\left.\frac{\partial\phi}{\partial y}\right|_d = \frac{\phi_0 - \phi_4}{h} \tag{3.128d}$$

The second-order derivatives are similarly approximated using these results as:

$$\left.\frac{\partial^2\phi}{\partial x^2}\right|_0 = \frac{1}{h}\left(\left.\frac{\partial\phi}{\partial x}\right|_c - \left.\frac{\partial\phi}{\partial x}\right|_a\right) \tag{3.129a}$$

$$= \frac{(\phi_3 - \phi_0) - (\phi_0 - \phi_1)}{h^2}$$

$$\left.\frac{\partial^2\phi}{\partial y^2}\right|_0 = \frac{1}{h}\left(\left.\frac{\partial\phi}{\partial y}\right|_b - \left.\frac{\partial\phi}{\partial y}\right|_d\right) \tag{3.129b}$$

$$= \frac{(\phi_2 - \phi_0) - (\phi_0 - \phi_4)}{h^2}$$

This amounts to a *central difference* expression for the partial derivatives [6]. Substituting these results into (3.127) gives a discrete approximation to Laplace's equation:

$$\frac{\partial^2\phi(x, y)}{\partial x^2} + \frac{\partial^2\phi(x, y)}{\partial y^2} = 0 \tag{3.130}$$

$$= \frac{\phi_1 + \phi_2 + \phi_3 + \phi_4 - 4\phi_0}{h^2}$$

or

$$\phi_0 = \tfrac{1}{4}[\phi_1 + \phi_2 + \phi_3 + \phi_4] \tag{3.131}$$

Thus the potential at a point is the average of the potentials of the surrounding 4 points in the mesh. Equation (3.131) is to be satisfied at all mesh points. Typically this is accomplished by prescribing the potentials of the mesh points on the conductor surfaces, initially prescribing zero potential to the interior points then recursively applying (3.131) at all the interior points until the change is less than some predetermined amount at which the iteration is terminated.

An example of the application of the method is shown in Fig. 3.44 which was solved earlier using a MOM method and a direct solution of Laplace's equation with those results given in Table 3.10. A rectangular box having the four conducting walls at different potentials is shown. The potentials of the interior mesh points obtained iteratively are shown. Observe that, even with this relatively course mesh, the potentials of the mesh points converge rather rapidly.

This method could also be solved in a direct fashion rather than iteratively. Enforcement of the potential via (3.131) at the six interior mesh points gives

TABLE 3.11 Comparison of the Finite Difference and Exact Results for the Potential in Fig. 3.30

	Direct method	Iteration	Exact
ϕ_a	16.44	16.41	16.478 4
ϕ_b	21.66	21.63	21.849 9
ϕ_c	14.10	14.07	14.157 5
ϕ_d	20.19	20.16	20.492 4
ϕ_e	9.77	9.76	9.609 42
ϕ_f	14.99	14.98	14.981 0

$$\begin{bmatrix} 4 & -1 & -1 & 0 & 0 & 0 \\ -1 & 4 & 0 & -1 & 0 & 0 \\ -1 & 0 & 4 & -1 & -1 & 0 \\ 0 & -1 & -1 & 4 & 0 & -1 \\ 0 & 0 & -1 & 0 & 4 & -1 \\ 0 & 0 & 0 & -1 & -1 & 4 \end{bmatrix} \begin{bmatrix} V_a \\ V_b \\ V_c \\ V_d \\ V_e \\ V_f \end{bmatrix} = \begin{bmatrix} 30 \\ 50 \\ 10 \\ 30 \\ 10 \\ 30 \end{bmatrix} \tag{3.132}$$

Solving this gives the potentials of the interior mesh points. Table 3.11 compares the results of the direct method with the iteration of Fig. 3.44 and with exact results obtained from an analytical solution of Laplace's equation given previously.

The solution for the potentials via this method is only one part of the process of determining the per-unit-length generalized capacitance matrix. In order to compute the generalized capacitance matrix, we need to determine the total charge on the conductors (per unit of line length). To implement this calculation, recall Gauss' law:

$$Q = \iint_s \vec{\mathscr{D}} \cdot d\vec{s} \tag{3.133}$$

which provides that the charge enclosed by a surface is equal to the integral of the normal component of the electric flux density vector over that surface. For a linear, homogeneous, isotropic medium,

$$\vec{\mathscr{D}} = \varepsilon \vec{\mathscr{E}} = \varepsilon \frac{\partial \phi}{\partial n} \hat{a}_n \tag{3.134}$$

where $\hat{a}_n$ is the unit vector normal to the surface. In order to apply this to the problem of computing the charge on the surface of a conductor, consider Fig. 3.45. Applying (3.133) and (3.134) to a strip along the conductor surface between the conductor and the first row of mesh points just off the surface gives

$$q = \oint_l \vec{\mathscr{D}} \cdot d\vec{l} = \oint_l \varepsilon \frac{\partial \phi}{\partial n} dl \tag{3.135}$$

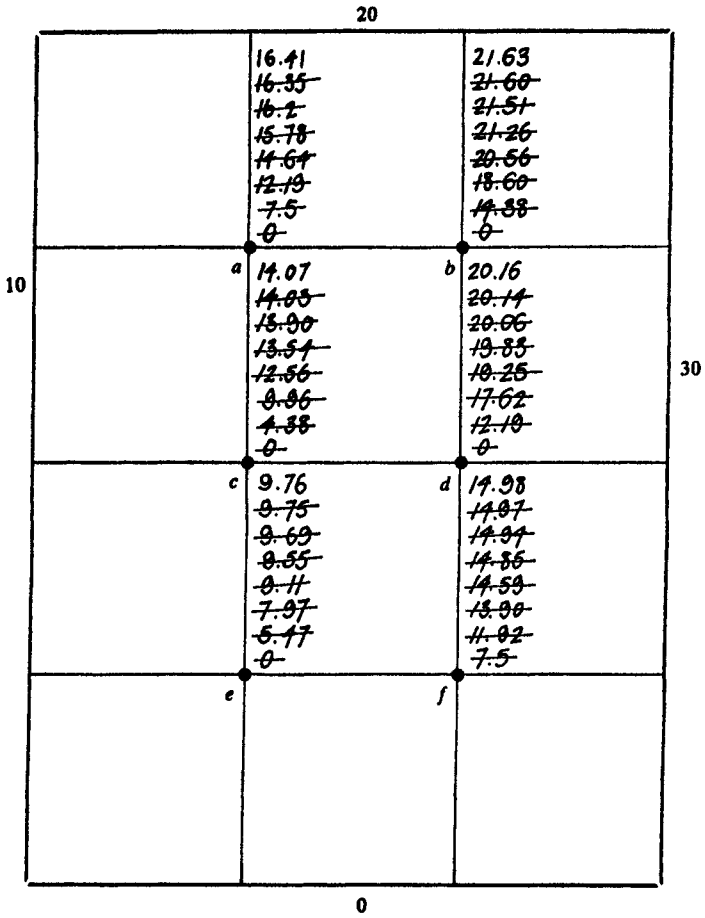

FIGURE 3.44 Example for illustration of the finite difference method.

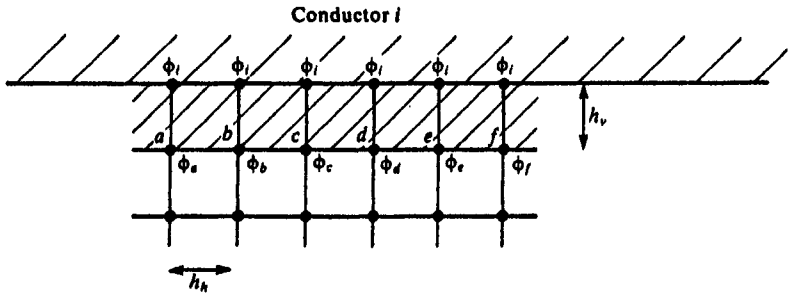

FIGURE 3.45 Use of the finite difference method in determining surface charge on a conductor.

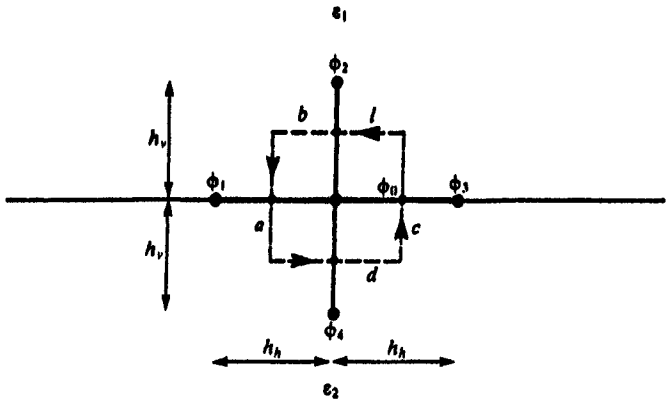

FIGURE 3.46 Illustration of the implementation of the finite difference method for multiple dielectrics.

Using the potentials computed at the interior mesh points, we can obtain the charge on the surface by applying (3.135) in discrete form as

$$q = \cdots + \varepsilon \frac{(\phi_i - \phi_a)}{h_v} h_h + \varepsilon \frac{(\phi_i - \phi_b)}{h_v} h_h + \varepsilon \frac{(\phi_i - \phi_c)}{h_v} h_h \qquad (3.136)$$
$$+ \varepsilon \frac{(\phi_i - \phi_d)}{h_v} h_h + \varepsilon \frac{(\phi_i - \phi_e)}{h_v} h_h + \varepsilon \frac{(\phi_i - \phi_f)}{h_v} h_h + \cdots$$

where h_v denotes the "vertical" length of the mesh perpendicular to the conductor surface, and h_h denotes the "horizontal" length of the mesh parallel to the conductor surface. Once the charges on the conductors are obtained in this fashion, the generalized capacitance matrix can be formed and from it the per-unit-length capacitances can be obtained.

Dielectric inhomogeneities can be handled in a similar fashion with this method. Gauss' law requires that, in the absence of any free charge intentionally placed at an interface between two dielectrics, there can be no net charge on the surface. Consider the interface between two dielectrics shown in Fig. 3.46 where a mesh has been assigned at the boundary. Applying Gauss' law to the surface surrounding the center point of the mesh shown as a dashed line gives

$$0 = \oint_l \vec{\mathcal{D}} \cdot d\vec{l} = \oint_l \varepsilon \frac{\partial \phi}{\partial n} dl \qquad (3.137)$$
$$= \varepsilon_1 \frac{(\phi_2 - \phi_0)}{h_v} h_h + \varepsilon_1 \frac{(\phi_1 - \phi_0)}{h_h} \frac{h_v}{2} + \varepsilon_2 \frac{(\phi_1 - \phi_0)}{h_h} \frac{h_v}{2}$$
$$+ \varepsilon_2 \frac{(\phi_4 - \phi_0)}{h_v} h_h + \varepsilon_2 \frac{(\phi_3 - \phi_0)}{h_h} \frac{h_v}{2} + \varepsilon_1 \frac{(\phi_3 - \phi_0)}{h_h} \frac{h_v}{2}$$

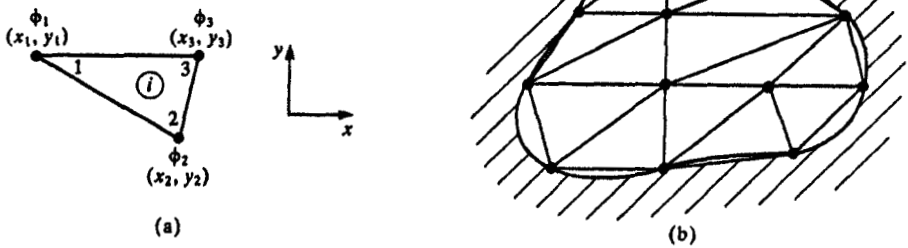

FIGURE 3.47 Illustration of (a) the finite element triangular element and (b) its use in representing two-dimensional problems.

Finite difference methods are particularly adapted to *closed systems.* For *open systems* where the space extends to infinity in all directions, a method must be employed to terminate the mesh. A rather simple but computationally intensive technique is to extend the mesh to a large but finite distance from the conductors and terminate it in zero potential. To check the sufficiency of this, extend the mesh slightly then recompute the results.

3.3.3 Finite Element Techniques

The third important numerical method for solving (approximately) Laplace's equation is the *finite element method* or FEM. The FEM approximates the region and its potential distribution by dividing the region into subregions (finite elements) and representing the potential distribution over that subregion. We will restrict our discussion to the most commonly used finite element, the triangle surface shown in Fig. 3.47(a). Higher-order elements are discussed in [6, 10]. Figure 3.47(b) illustrates the approximation of a two-dimensional region using these triangular elements. The triangular element has three nodes at which the potentials are prescribed (known). The potential distribution over the element is a polynomial approximation in the x, y coordinates.

$$\phi(x, y) = a + bx + cy \tag{3.138}$$

Evaluating this equation at the three nodes gives

$$\begin{bmatrix} \phi_1 \\ \phi_2 \\ \phi_3 \end{bmatrix} = \begin{bmatrix} 1 & x_1 & y_1 \\ 1 & x_2 & y_2 \\ 1 & x_3 & y_3 \end{bmatrix} \begin{bmatrix} a \\ b \\ c \end{bmatrix} \tag{3.139}$$

Solving this for the coefficients gives

$$a = \frac{1}{2A}[K_1\phi_1 + K_2\phi_2 + K_3\phi_3] \tag{3.140a}$$

$$b = \frac{1}{2A}[Y_1\phi_1 + Y_2\phi_2 + Y_3\phi_3] \tag{3.140b}$$

$$c = -\frac{1}{2A}[X_1\phi_1 + X_2\phi_2 + X_3\phi_3] \tag{3.140c}$$

where

$$\left.\begin{aligned} K_1 &= (x_2y_3 - x_3y_2) \\ K_2 &= (x_3y_1 - x_1y_3) \\ K_3 &= (x_1y_2 - x_2y_1) \end{aligned}\right\} \tag{3.140d}$$

$$\left.\begin{aligned} Y_1 &= (y_2 - y_3) \\ Y_2 &= (y_3 - y_1) \\ Y_3 &= (y_1 - y_2) \end{aligned}\right\} \tag{3.140e}$$

$$\left.\begin{aligned} X_1 &= (x_2 - x_3) \\ X_2 &= (x_3 - x_1) \\ X_3 &= (x_1 - x_2) \end{aligned}\right\} \tag{3.140f}$$

and the area of the element is

$$A = \frac{1}{2}\begin{vmatrix} 1 & x_1 & y_1 \\ 1 & x_2 & y_2 \\ 1 & x_3 & y_3 \end{vmatrix} \tag{3.141}$$

$$= \tfrac{1}{2}[K_1 + K_2 + K_3]$$

Observe the cyclic ordering of the subscripts in (3.140) as $1 \to 2 \to 3$. Given the node potentials, the potential at points on the element surface can be found from (3.138) using (3.140) and (3.141). The electric field over the surface of the element is constant:

$$\vec{E} = -\nabla\phi \tag{3.142}$$

$$= -b\hat{a}_x - c\hat{a}_y$$

Observe that when a surface is approximated by these triangular elements as in Fig. 3.47(b), the potential is guaranteed to be continuous across the common boundaries between any adjacent elements.

The key feature in insuring a solution of Laplace's equation by this method is that the solution is such that *the total energy in the field distribution in the region is a minimum* [6, 10]. The total energy in the system is the sum of the energies of the elements:

$$W = \sum_{i=1}^{N_t} W^{(i)} \tag{3.143}$$

The minimum energy requirement is that the derivatives with respect to all *free nodes* (nodes where the potential is unknown) are zero:

$$\left.\frac{\partial W}{\partial \phi_i}\right|_{\text{all free nodes}} = 0 \tag{3.144}$$

The energy of the i-th element is

$$\begin{aligned} W^{(i)} &= \frac{1}{2}\int_{s_i} \varepsilon_i |\vec{E}_i|^2 \, ds_i \qquad (3.145)\\ &= \frac{\varepsilon_i}{2}\int_{s_i} (b_i^2 + c_i^2)\, ds_i \\ &= \frac{\varepsilon_i}{2}(b_i^2 + c_i^2) A_i \\ &= \frac{\varepsilon_i}{8A_i}[(Y_{i1}^2 + X_{i1}^2)\phi_1^{(i)}\phi_1^{(i)} + 2(Y_{i1}Y_{i2} + X_{i1}X_{i2})\phi_1^{(i)}\phi_2^{(i)} \\ &\quad + (Y_{i2}^2 + X_{i2}^2)\phi_2^{(i)}\phi_2^{(i)} + 2(Y_{i1}Y_{i3} + X_{i1}X_{i3})\phi_1^{(i)}\phi_3^{(i)} \\ &\quad + (Y_{i3}^2 + X_{i3}^2)\phi_3^{(i)}\phi_3^{(i)} + 2(Y_{i2}Y_{i3} + X_{i2}X_{i3})\phi_2^{(i)}\phi_3^{(i)} \end{aligned}$$

where $\phi_k^{(i)}$ is the potential of node k ($k = 1, 2, 3$) for the i-th element. This can be written in matrix notation as a *quadratic form* as

$$W^{(i)} = \tfrac{1}{2}\boldsymbol{\phi}^{(i)t}\mathbf{C}^{(i)}\boldsymbol{\phi}^{(i)} \tag{3.146a}$$

where

$$\boldsymbol{\phi}^{(i)} = \begin{bmatrix} \phi_1^{(i)} \\ \phi_2^{(i)} \\ \phi_3^{(i)} \end{bmatrix} \tag{3.146b}$$

and superscript t denotes transpose. The matrix

$$\mathbf{C}^{(i)} = \begin{bmatrix} C_{11}^{(i)} & C_{12}^{(i)} & C_{13}^{(i)} \\ C_{12}^{(i)} & C_{22}^{(i)} & C_{23}^{(i)} \\ C_{13}^{(i)} & C_{23}^{(i)} & C_{33}^{(i)} \end{bmatrix} \tag{3.146c}$$

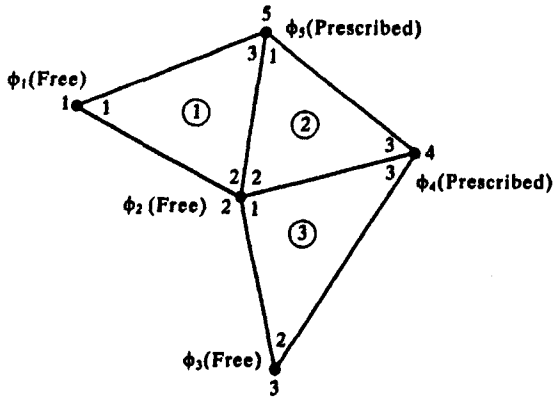

FIGURE 3.48 An example to illustrate the use of the FEM.

is referred to as the *local coefficient matrix* with entries

$$C_{mn}^{(l)} = \frac{\delta_l}{4A_l}(Y_{lm}Y_{ln} + X_{lm}X_{ln}) \tag{3.146d}$$

Now we must assemble the total energy expression for a system which is approximated by finite elements according to (3.143). In order to illustrate this consider the example of a region that is represented by three finite elements shown in Fig. 3.48. The node numbers inside the elements are the *local node numbers* as used above. The *global node numbers* are shown uniquely for the five nodes. Nodes 1, 2, and 3 are *free nodes* whose potential is to be determined to satisfy Laplace's equation in the region. Nodes 4 and 5 are *prescribed nodes* whose potentials are fixed (known). The total energy expression can be written in terms of the global nodes as

$$W = \sum_{l=1}^{N_e} W^{(l)} \tag{3.147a}$$

$$= \tfrac{1}{2}\boldsymbol{\phi}^t \mathbf{C} \boldsymbol{\phi}$$

where the vector of global node potentials is

$$\boldsymbol{\phi} = \begin{bmatrix} \phi_1 = \phi_1^{(1)} \\ \phi_2 = \phi_2^{(1)} = \phi_2^{(2)} = \phi_1^{(3)} \\ \phi_3 = \phi_2^{(3)} \\ \phi_4 = \phi_3^{(2)} = \phi_3^{(3)} \\ \phi_5 = \phi_3^{(1)} = \phi_1^{(2)} \end{bmatrix} \tag{3.147b}$$

and

$$\mathbf{C} = \begin{bmatrix} C_{11} & C_{12} & C_{13} & C_{14} & C_{15} \\ C_{12} & C_{22} & C_{23} & C_{24} & C_{25} \\ C_{13} & C_{23} & C_{33} & C_{34} & C_{35} \\ C_{14} & C_{24} & C_{34} & C_{44} & C_{45} \\ C_{15} & C_{25} & C_{35} & C_{45} & C_{55} \end{bmatrix} \tag{3.147c}$$

This *global coefficient matrix*, **C**, like the local coefficient matrix, can be shown to be symmetric by energy considerations [A.1]. The entries in the global coefficient matrix can be assembled quite easily from the local coefficient matrix (whose entries are computed for the isolated elements independent of their future connection) with the following observation. For each element write the global coefficient matrix as

$$W^{(1)} = \boldsymbol{\phi}^t \begin{bmatrix} C_{11}^{(1)} & C_{12}^{(1)} & 0 & 0 & C_{13}^{(1)} \\ C_{12}^{(1)} & C_{22}^{(1)} & 0 & 0 & C_{23}^{(1)} \\ 0 & 0 & 0 & 0 & 0 \\ 0 & 0 & 0 & 0 & 0 \\ C_{13}^{(1)} & C_{23}^{(1)} & 0 & 0 & C_{33}^{(1)} \end{bmatrix} \boldsymbol{\phi} \tag{3.148a}$$

$$W^{(2)} = \boldsymbol{\phi}^t \begin{bmatrix} 0 & 0 & 0 & 0 & 0 \\ 0 & C_{22}^{(2)} & 0 & C_{23}^{(2)} & C_{12}^{(2)} \\ 0 & 0 & 0 & 0 & 0 \\ 0 & C_{23}^{(2)} & 0 & C_{33}^{(2)} & C_{13}^{(2)} \\ 0 & C_{12}^{(2)} & 0 & C_{13}^{(2)} & C_{11}^{(2)} \end{bmatrix} \boldsymbol{\phi} \tag{3.148b}$$

$$W^{(3)} = \boldsymbol{\phi}^t \begin{bmatrix} 0 & 0 & 0 & 0 & 0 \\ 0 & C_{11}^{(3)} & C_{12}^{(3)} & C_{13}^{(3)} & 0 \\ 0 & C_{12}^{(3)} & C_{22}^{(3)} & C_{23}^{(3)} & 0 \\ 0 & C_{13}^{(3)} & C_{23}^{(3)} & C_{33}^{(3)} & 0 \\ 0 & 0 & 0 & 0 & 0 \end{bmatrix} \boldsymbol{\phi} \tag{3.148c}$$

Assembling these according to (3.147) gives the total energy:

$$W = W^{(1)} + W^{(2)} + W^{(3)}$$

$$= \boldsymbol{\phi}^t \begin{bmatrix} C_{11}^{(1)} & C_{12}^{(1)} & 0 & 0 & C_{13}^{(1)} \\ C_{12}^{(1)} & C_{22}^{(1)} + C_{22}^{(2)} + C_{11}^{(3)} & C_{12}^{(3)} & C_{23}^{(2)} + C_{13}^{(3)} & C_{23}^{(1)} + C_{12}^{(2)} \\ 0 & C_{12}^{(3)} & C_{22}^{(3)} & C_{23}^{(3)} & 0 \\ 0 & C_{23}^{(2)} + C_{13}^{(3)} & C_{23}^{(3)} & C_{33}^{(2)} + C_{33}^{(3)} & C_{13}^{(2)} \\ C_{13}^{(1)} & C_{23}^{(1)} + C_{12}^{(2)} & 0 & C_{13}^{(2)} & C_{33}^{(1)} + C_{11}^{(2)} \end{bmatrix} \boldsymbol{\phi} \tag{3.149}$$

A very simple rule for assembling this global coefficient matrix can be developed from this example. *The main diagonal terms are the sums of the main diagonal terms of the local coefficient matrices for those elements that connect to this global node. The off-diagonal terms are the sums of the off-diagonal terms of the local coefficient matrices whose sides connect the two global nodes.* Observe that the off-diagonal terms will have at most two entries, whereas the main diagonal terms will be the sum of a number of terms equal to the number of elements that share the global node.

Now it remains to differentiate this result with respect to the free nodes to insure minimum energy of the system thereby satisfying Laplace's equation. To that end let us number the global nodes by numbering the free nodes first and then numbering the prescribed (fixed potential) nodes last. The above energy expression can then be written in partitioned form as

$$W = \tfrac{1}{2}[\phi_f^t \quad \phi_p^t]\begin{bmatrix} \mathbf{C}_{ff} & \mathbf{C}_{fp} \\ \mathbf{C}_{pf} & \mathbf{C}_{pp} \end{bmatrix}\begin{bmatrix} \phi_f \\ \phi_p \end{bmatrix} \tag{3.150}$$

$$= \tfrac{1}{2}[\phi_f^t \mathbf{C}_{ff}\phi_f + \phi_f^t \mathbf{C}_{fp}\phi_p + \phi_p^t \mathbf{C}_{pf}\phi_f + \phi_p^t \mathbf{C}_{pp}\phi_p]$$

Differentiating this with respect to the free node potentials and setting the result to zero gives the final equations to be solved:

$$\mathbf{C}_{ff}\phi_f = -\mathbf{C}_{fp}\phi_p \tag{3.151}$$

Solving this matrix equation for the free node potentials is referred to as the *direct method* of solving the FEM equations.

Observe from the example of Fig. 3.48 that the global coefficient matrix, C, has a number of zero entries. This is quite evident since only those (two) elements that contain the nodes for this entry will contribute a nonzero term. Thus the coefficient matrices in (3.151) will be *sparse*. Although there exist sparse matrix solution routines which efficiently take advantage of this, FEM problems, particularly large ones, are generally solved more efficiently using the *iterative method*. This is similar to the iterative method for the finite difference technique in that the free nodes are initially prescribed some starting value (such as zero) and the new values of the free node potentials computed. The process continues until the change in the free node potentials between iteration steps is less than some value. Writing out (3.151) for the example of Fig. 3.48 gives

$$\begin{bmatrix} C_{11} & C_{12} & C_{13} \\ C_{12} & C_{22} & C_{23} \\ C_{13} & C_{23} & C_{33} \end{bmatrix}\begin{bmatrix} \phi_1 \\ \phi_2 \\ \phi_3 \end{bmatrix} + \begin{bmatrix} C_{14} & C_{15} \\ C_{24} & C_{25} \\ C_{34} & C_{35} \end{bmatrix}\begin{bmatrix} \phi_4 \\ \phi_5 \end{bmatrix} = \begin{bmatrix} 0 \\ 0 \\ 0 \end{bmatrix} \tag{3.152}$$

Writing each free potential in terms of the other free potentials and the

prescribed potentials gives

$$\boldsymbol{\phi}_f^{\text{new}} = -\begin{bmatrix} 0 & C_{12}/C_{11} & C_{13}/C_{11} \\ C_{12}/C_{22} & 0 & C_{23}/C_{22} \\ C_{13}/C_{33} & C_{23}/C_{33} & 0 \end{bmatrix} \boldsymbol{\phi}_f^{\text{old}} + \begin{bmatrix} C_{14}/C_{11} & C_{15}/C_{11} \\ C_{24}/C_{22} & C_{25}/C_{22} \\ C_{34}/C_{33} & C_{35}/C_{33} \end{bmatrix} \boldsymbol{\phi}_p \quad (3.153a)$$

where

$$\boldsymbol{\phi} = \begin{bmatrix} \phi_1 \\ \phi_2 \\ \phi_3 \end{bmatrix} \quad (3.153b)$$

$$\boldsymbol{\phi}_p = \begin{bmatrix} \phi_4 \\ \phi_5 \end{bmatrix} \quad (3.153c)$$

As a numerical illustration of the method consider the problem of a rectangular region of sides lengths 4 and 3 with prescribed potentials of 0V, 10V, 20V, and 30V as shown in Fig. 3.30. This was solved earlier with the MOM technique and the finite difference technique. In order to compare this with the finite difference technique we will again choose six interior nodes and approximate the space between these nodes with twenty-four finite elements as shown in Fig. 3.49. Observe that the potentials at nodes 7, 10, 14, and 17 are not known since these are gaps between the adjacent conductors. We will prescribe these potentials as the average of the adjacent conductor potentials: 5V, 15V, 25V, and 15V. The solution for the six interior node potentials via the direct and the iterative method are given in Table 3.12. The iterative method converged after fifteen iterations.

Some of the important features of the FEM are that it can handle irregular boundaries as well as inhomogeneous media. Inhomogeneous media are handled by insuring that the region is subdivided such that each finite element covers (approximately) a homogeneous subregion. The permittivities of the finite elements, ε_l, are contained in the $C_{mn}^{(l)}$ local node coefficients.

TABLE 3.12 Comparison of the Finite Element and Exact Results for the Potential in Fig. 3.30

	Direct method	Iteration	Exact
ϕ_1	16.438 9	16.438 9	16.478 4
ϕ_2	21.656 3	21.656 3	21.849 9
ϕ_3	14.099 4	14.099 4	14.157 5
ϕ_4	20.186 3	20.186 3	20.492 4
ϕ_5	9.772 26	9.772 24	9.609 42
ϕ_6	14.989 6	14.989 6	14.981 0

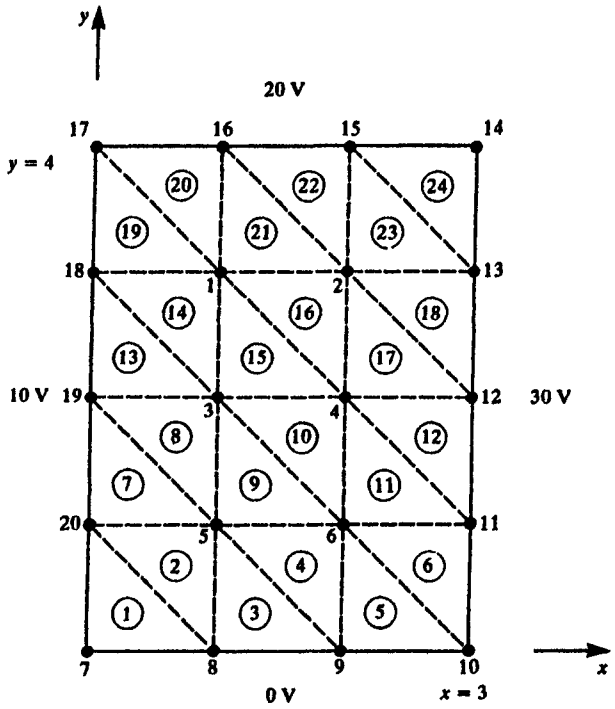

FIGURE 3.49 Illustration of the FEM applied to a previously solved problem.

Once again, as with the finite difference method, the finite element method is most suited to closed systems. For open systems whose boundaries extend to infinity, an infinite mesh method can be developed [6] or the mesh can be extended sufficiently far from the main areas of interest and artificially terminated in zero potential thereby forming a closed system, albeit an artificial one.

The FEM is a highly versatile method for solving Laplace's equation as well as other electromagnetic fields problems [6, 10]. Other parameters of interest such as capacitances can be determined in the usual fashion by determining the resulting charge on the conductors as the normal component of the displacement vector just off the conductor surfaces.

3.4 MISCELLANEOUS ADDITIONAL TECHNIQUES

The previous sections have discussed methods for determining the per-unit-length capacitances (and implicitly inductances) via approximate methods. The only structures for which these parameters yielded exact solutions were for the cases:

1. Two wires in a homogeneous medium.

2. One wire in a homogeneous medium above an infinite, perfectly conducting plane.
3. One wire within and located on the axis of an overall shield with the dielectric having symmetry about that axis.

There exist similar closed-form solutions for infinite, periodic structures of wires [11]. There also exist some analytical solutions for structures that consist of rectangular-cross-section conductors in inhomogeneous media (lands on PCB's) [12]. But these are restricted to *only two conductors.* However, for the structures that exhibit crosstalk, there must exist more than two conductors and the number is finite. Furthermore, these structures typically are surrounded by an inhomogeneous medium. Thus the feasible way of determining the entries in the per-unit-length parameter matrices is through numerical methods discussed previously. Although not as useful for multiconductor lines as the previously discussed numerical methods, there are some additional solution techniques that are worth noting. These methods are the conformal mapping technique and the spectral-domain technique which will be briefly discussed in this section.

3.4.1 Conformal Mapping Techniques

Conformal mapping techniques seek to transform the desired two-dimensional geometry to another geometry which is easier to solve [11–14]. It is desired to obtain a transformation of variables that map the original x, y coordinates over to some other u, v coordinate system as

$$u = u(x, y) \tag{3.154a}$$

$$v = v(x, y) \tag{3.154b}$$

The transformation is represented as

$$W = u + jv = F(Z = x + jy) \tag{3.155}$$

The function F must be an analytic function of Z, $dW/dZ = dF/dZ$, in order that the capacitance of both structures is identical [13]. The function F will be guaranteed to be analytic if u and v satisfy the Cauchy–Riemann equations:

$$\frac{\partial u}{\partial x} = \frac{\partial v}{\partial y} \tag{3.156a}$$

$$\frac{\partial u}{\partial y} = -\frac{\partial v}{\partial x} \tag{3.156b}$$

Finding the appropriate transformation that simplifies the problem is, of course, the crucial issue with this method but it has been successfully applied to various PCB-type structures [12, 14].

3.4.2 Spectral-Domain Techniques

There are various versions of the so-called *spectral-domain method.* Our interest here is in the applications to the solution of the two-dimensional Laplace equation:

$$\nabla^2\phi(x, y) = \frac{\partial^2\phi}{\partial x^2} + \frac{\partial^2\phi}{\partial y^2} = 0 \tag{3.157}$$

Take the Fourier transform of ϕ with respect to x or y. Typically we transform with respect to the variable that should not require imposition of a boundary condition. For example, if we label the axis parallel to a PCB as the x axis (along which the structure is infinite in length) and the axis perpendicular to the PCB as the y axis (along which boundary conditions will be imposed), we would transform with respect to x as

$$\hat{\phi}(\beta, y) = \int_{-\infty}^{\infty} \phi(x, y)e^{j\beta x}\,dx \tag{3.158}$$

Laplace's partial differential equation when transformed becomes an *ordinary differential equation*:

$$\frac{d^2\hat{\phi}(\beta, y)}{dy^2} - \beta^2\hat{\phi}(\beta, y) = 0 \tag{3.159}$$

Which has the simple solution

$$\hat{\phi}(\beta, y) = Ae^{-\beta y} + Be^{\beta y} \tag{3.160}$$

where A and B are, as yet, undetermined constants. Represent the charge distribution over the conductor surfaces as $f(x)$ so that the total charge on a conductor is

$$Q = \int_{-\infty}^{\infty} f(x)\,dx \tag{3.161}$$

Applying the boundary conditions (in the y variable) to (3.160) to determine A and B, it can be shown, using Parseval's theorem, that the capacitance of a two-conductor system becomes simply [15]

$$\frac{1}{C} = \frac{1}{2\pi Q^2}\int_{-\infty}^{\infty} \hat{f}(\beta)\hat{\phi}(\beta, y = \text{conductor})\,d\beta \tag{3.162}$$

One advantage of this method is that the capacitance can be found from (3.162) without the need to determine the inverse Fourier transform of $\hat{\phi}(\beta, y)$. The other advantage is that this is a variational method so that a relatively crude

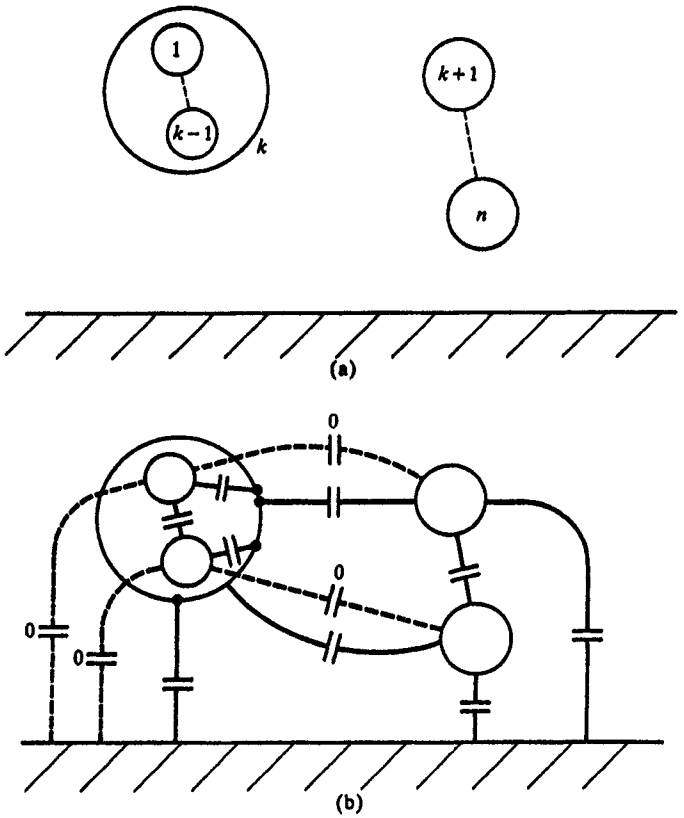

FIGURE 3.50 Electrostatic isolation of two regions by a shield: (a) problem definition and (b) illustration of the resulting capacitances.

approximation to the charge distribution, $f(x)$, will yield very accurate results for the capacitance of the structure.

3.5 SHIELDED LINES

Some MTL's have a subset of the conductors completely surrounded by a perfectly conducting *shield* as illustrated in Fig. 3.50(a). The shield separates $k-1$ of the conductors *electrostatically* from the remaining set. The electric field lines of the conductors internal to the shield terminate on the interior of the shield, and the electric field lines of the conductors external to the shield terminate on the exterior of the shield. This shows that the mutual capacitances and self-capacitances between conductors interior and exterior to the shield will

be zero as illustrated in Fig. 3.50(b) [I.2]. Therefore, the determination of the overall per-unit-length capacitance matrix is broken into two separate solutions and the overall capacitance matrix has the form

$$\mathbf{C} = \begin{bmatrix} \mathbf{C}_i & \mathbf{0} \\ \mathbf{0} & \mathbf{C}_o \end{bmatrix} \tag{3.163}$$

where $\mathbf{C}_i$ is the $(k-1) \times (k-1)$ per-unit-length capacitance matrix of the system of $k-1$ conductors within the shield, and $\mathbf{C}_o$ is the $(n-k+1) \times (n-k+1)$ per-unit-length capacitance matrix of the system of conductors external to the shield (including, in the case of a ground plane, the shield). If we assume that the shield is not ferromagnetic, $\mu_r = 1$, then the per-unit-length inductance has inductances between all conductors of the system and is full:

$$\mathbf{L} = \begin{bmatrix} \mathbf{L}_i & \mathbf{L}_{io} \\ \mathbf{L}_{io} & \mathbf{L}_o \end{bmatrix} \tag{3.164}$$

If the two media within and without the shield are individually homogeneous, ε_{ri}, μ and ε_{ro}, μ, the various inductance and capacitance submatrices are related by

$$\mathbf{C}_i\mathbf{L}_i = \mu\varepsilon_o\varepsilon_{ri}\mathbf{1}_{k-1} \tag{3.165a}$$

and

$$\mathbf{C}_o\mathbf{L}_o = \mu\varepsilon_o\varepsilon_{ro}\mathbf{1}_{n-k+1} \tag{3.165b}$$

This simplifies the determination of the per-unit-length parameter submatrices and has been implemented in various computer codes. Shields inherently enclose electric fields and limit electrostatic coupling. They do not, however, inherently restrict or eliminate magnetostatic coupling unless some additional provision is made, as when the shield is grounded at both ends to allow a current to flow along the shield thereby generating a counteracting magnetic flux [A.3]. These concepts are implemented in the FORTRAN program **SHIELD** for computing crosstalk between individually shielded cables that is described in [I.2, I.3].

3.6 INCORPORATION OF LOSSES; CALCULATION OF R, L_i, AND G

The remaining parameters, the entries in the per-unit-length resistance matrix, R, and the per-unit-length conductance matrix, G, provide the line loss. In addition, the currents of imperfect conductors do not flow solely on the conductor surfaces as with perfect conductors but are distributed over the conductor cross sections. This gives rise to a portion of the per-unit-length inductance matrix, the internal inductance, L_i, due to magnetic flux internal to the conductors. This can be included in the total per-unit-length inductance

matrix as $\mathbf{L} = \mathbf{L}_i + \mathbf{L}_e$ where $\mathbf{L}_e$ is the external inductance due to magnetic flux external to the conductors. We have previously assumed perfect conductors wherein $\mathbf{L} = \mathbf{L}_e$.

3.6.1 Calculation of the Per-Unit-Length Conductance Matrix, G

If the surrounding medium is *homogeneous*, G can be obtained from C or L as described earlier:

$$\mathbf{G} = \frac{\sigma}{\varepsilon}\mathbf{C} = \mu\sigma\mathbf{L}^{-1} \tag{3.166}$$

and $\mathbf{L} = \mathbf{L}_e$ is the external inductance matrix assuming perfect conductors. So the difficulty in obtaining G arises for *inhomogeneous media*. Actually, this turns out to be a simple modification of the calculation of the per-unit-length capacitance matrix, C (also computed assuming perfect conductors). Losses in the medium are due to:

1. Conductive losses due to the conductance parameter, σ.
2. Polarization losses as described previously.

Both of these losses can be represented by a complex permittivity. This can be readily seen by writing Ampere's law for sinusoidal excitation as [A.1]

$$\begin{aligned}\nabla \times \vec{H} &= (\sigma + j\omega(\varepsilon - j\varepsilon_b))\vec{E} \\ &= j\omega\left(\varepsilon - j\left(\varepsilon_b + \frac{\sigma}{\omega}\right)\right)\vec{E} \\ &= j\omega\underbrace{(\varepsilon' - j\varepsilon'')}_{\hat{\varepsilon}}\vec{E}\end{aligned} \tag{3.167}$$

where ε_b represents the polarization loss due to bound charge and σ represents the conduction current losses due to free charge in the dielectric. All of these parameters, ε, ε_b, σ, are functions of frequency to varying degrees. Typically ε is relatively independent of frequency up to frequencies in the low gigahertz range and ranges from $2\varepsilon_o$ to $20\varepsilon_o$. Ordinarily there is little free charge in typical dielectrics, and the loss is due to polarization loss which is normally significant only above the low gigahertz range of frequencies. In any event we may represent both loss mechanisms by using a complex permittivity $\hat{\varepsilon} = \varepsilon' - j\varepsilon''$ where

$$\varepsilon' = \varepsilon \tag{3.168a}$$

$$\begin{aligned}\varepsilon'' &= \varepsilon_b + \frac{\sigma}{\omega} \\ &= \varepsilon' \tan\delta\end{aligned} \tag{3.168b}$$

The real and imaginary parts of the complex dielectric constant, ε' and ε'', are not independent but are related by the Kramers–Kronig relations [16]. The term $\tan\delta$ is referred to as the *loss tangent* and is tabulated for various materials and at various frequencies in numerous handbooks [17]. The result in (3.167) shows that *we can include losses in the medium by solving for the capacitance matrix for a medium having a complex permittivity,* $\hat{\varepsilon} = \varepsilon'(1 - j\tan\delta)$, *and from that result directly obtain* **C** *and* **G**. To show this write the per-unit-length admittance matrix as

$$\hat{\mathbf{Y}} = \mathbf{G} + j\omega\mathbf{C} \tag{3.169}$$

$$= j\omega\left(\mathbf{C} - j\frac{1}{\omega}\mathbf{G}\right)$$

$$= j\omega(\hat{\mathbf{C}} = \mathbf{C}_R + j\mathbf{C}_I)$$

This shows that we could determine the capacitance matrix $\hat{\mathbf{C}}$ using a complex permittivity $\hat{\varepsilon} = \varepsilon(1 - j\tan\delta)$ and obtain

$$\mathbf{C} = \mathbf{C}_R \tag{3.170a}$$

$$= \mathscr{R}e(\hat{\mathbf{C}})$$

$$\mathbf{G} = -\omega\mathbf{C}_I \tag{3.170b}$$

$$= -\omega\mathscr{I}m(\hat{\mathbf{C}})$$

This is a standard idea used for many years to include losses in media [A.1]. It also applies to *inhomogeneous media if we use the complex permittivities of the various homogeneous regions in computing the complex capacitance matrix,* $\hat{\mathbf{C}}$, [B.1, 18–2]! It is a simple matter to modify the **RIBBON.FOR, PCB.FOR,** and **PCBGAL.FOR** codes described in Appendix A for computing the per-unit-length capacitance matrices of inhomogeneous, lossy media. Simply declare the permittivity (and all quantities involving it) to be complex, provide the loss tangent *at the frequency of interest* as input and use a complex equation solver instead of a real equation solver. The generalized capacitance matrix will be complex from which $\hat{\mathbf{C}}$ can be determined in the usual fashion. Then **C** and **G** can be extracted from that result according to (3.170). Table 3.13 gives results for the three-wire ribbon cable considered previously, this time assuming a loss tangent at 100 MHz of $\tan\delta = 0.01$. A value of loss tangent of $\tan\delta = 0.01$ at 100 MHz is somewhat unrealistically large for typical insulation materials (polyvinyl chloride) at 100 MHz. However, the entries in **G** are still substantially less than those of $\omega\mathbf{C}$ at 100 MHz by over two orders of magnitude (a factor of the order of 300) so the dielectric loss is not significant. The entries in **G** are not substantially different for a loss tangent of $\tan\delta = 0.001$ further indicating this is a low-loss situation.

For typical dielectrics and dimensions of MTL's it is frequently possible to neglect **G**, i.e., set $\mathbf{G} = \mathbf{0}$. In order to illustrate the reasonable nature of this

TABLE 3.13 The Transmission-Line Capacitances and Conductances for the Three-Wire Ribbon Cable (tan δ = 0.01, 100 MHz)

Entry	C, without loss (pF/m)	C, with loss (pF/m)	G (μS/m)
11	37.432	37.432	64.763
12	−18.716	−18.716	−32.381
22	24.982	24.982	34.722

approximation and to bound the error incurred by neglecting **G**, suppose that the medium is *homogeneous*. The capacitance matrix for this lossless, homogeneous medium is related to a constant matrix that is dependent only on the cross-sectional dimensions as

$$\mathbf{C} = \varepsilon \mathbf{K} \tag{3.171}$$

The conductance matrix is similarly related to **K** for this lossy, homogeneous medium. Substituting the complex permittivity into (3.171) yields the per-unit-length admittance as

$$\begin{aligned} \hat{\mathbf{Y}} &= j\omega\hat{\mathbf{C}} \\ &= j\omega\varepsilon'(1 - j\tan\delta)\mathbf{K} \\ &= \underbrace{\omega\varepsilon'\tan\delta\mathbf{K}}_{\mathbf{G}} + \underbrace{j\omega\varepsilon'\mathbf{K}}_{\mathbf{C}} \end{aligned} \tag{3.172}$$

from which we obtain

$$\mathbf{G} = \omega\tan\delta\mathbf{C} \tag{3.173}$$

If the loss tangent is constant, the entries in the per-unit-length conductance matrix, **G**, increase directly with frequency. The importance of **G** can be bounded by realizing that the entries in **G** will be added to the entries in $j\omega\mathbf{C}$ to give the total per-unit-length admittance matrix

$$\begin{aligned} \hat{\mathbf{Y}} &= \mathbf{G} + j\omega\mathbf{C} \\ &= \omega(\tan\delta + j1)\mathbf{C} \end{aligned} \tag{3.174}$$

In the case of an *inhomogeneous medium* the entries in **G** can be no larger than (3.173) using the *largest loss tangent* for all the various media of the problem. Thus, *for a lossy inhomogeneous medium, the entries in* **G** *will be negligible in comparison to the entries in* $\omega\mathbf{C}$ *and can therefore be neglected if the largest loss tangent of all the various media is several orders of magnitude less than unity*! This is typically (but not always) the case in practical situations. Molecular

resonances in the microwave range can lead to large loss tangents over certain frequency bands [21]. For example, for dielectrics used in typical MTL's (ribbon cables, coupled microstrips, PCB's, etc.), the loss tangent below the low gigahertz frequency range is of the order of 10^{-4} [16, 17]. For silicon substrates used in typical microstrip lines, the loss tangent is of the order of 2.5×10^{-4}. Observe that the *reciprocals* of the entries in G represent resistances between each conductor and between each conductor and the reference conductor which carry the transverse conduction currents. The entries in G are of the order of 10^{-3} S/m to 10^{-4} S/m which represent transverse resistances of some 1 kΩ to 10 kΩ between conductors. Use of values of entries in G considerably larger than this are not representative of *useful* transmission-line structures. Thus for typical MTL's and for frequencies up to the low gigahertz range, neglecting G, setting $\mathbf{G} = \mathbf{0}$, typically does not appreciably affect the solutions for the line terminal voltages and currents.

3.6.2 Representation of Conductor Losses

In contrast to losses in the surrounding medium, losses due to imperfect line conductors may be significant even for frequencies below the low gigahertz range. These losses are determined by the entries in the per-unit-length resistance matrix, R. At low frequencies, the entries in R are constant, whereas at the higher frequencies they typically vary as the square root of frequency, $\sqrt{f}$, as a result of *skin effect*. Also the imperfect conductors give rise to internal inductances which contribute to $\mathbf{L}_i$. These elements typically are constant at low frequencies and *decrease* as $\sqrt{f}$ at the higher frequencies. Thus at the higher frequencies their inductive reactances, $\omega\mathbf{L}_i$, *increase* as $\sqrt{f}$, whereas the external inductive reactances, $\omega\mathbf{L}_e$, *increase* as f.

The current density and the electric and magnetic fields in good conductors are governed by the *diffusion equation*. Ampere's law relates the magnetic field to the sum of conduction current and displacement current as

$$\nabla \times \vec{H} = \underbrace{\sigma\vec{E}}_{\text{conduction}} + \underbrace{j\omega\varepsilon\vec{E}}_{\text{displacement}} \tag{3.175}$$

A good conductor is one in which the conduction current (which implicitly includes the polarization loss) greatly exceeds the displacement current which is satisfied for most metallic conductors and frequencies of reasonable interest. Thus Ampere's law within the conductor becomes approximately

$$\nabla \times \vec{H} \cong \vec{J} = \sigma\vec{E} \tag{3.176a}$$

Similarly, Faraday's law is

$$\nabla \times \vec{E} = -j\omega\mu\vec{H} \tag{3.176b}$$

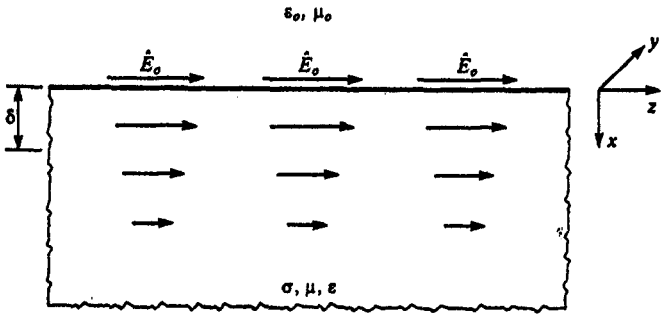

FIGURE 3.51 Diffusion of currents and fields into a semi-infinite conductive half-space.

Taking the curl of Faraday's law gives [A.1]

$$\nabla \times \nabla \times \vec{\hat{E}} = \nabla(\nabla \cdot \vec{\hat{E}}) - \nabla^2 \vec{\hat{E}} = -j\omega\mu \nabla \times \vec{\hat{H}} \tag{3.177}$$

Substituting Gauss' law:

$$\nabla \cdot \varepsilon_o \vec{\hat{E}} = 0 \tag{3.178}$$

gives

$$\nabla^2 \vec{\hat{E}} = j\omega\mu\sigma \vec{\hat{E}} \tag{3.179}$$

Since the current density is related to the electric field in the conductor as $\vec{\hat{J}} = \sigma \vec{\hat{E}}$, we arrive at the *diffusion equation*:

$$\nabla^2 \vec{\hat{J}} = j\omega\mu\sigma \vec{\hat{J}} \tag{3.180}$$

3.6.2.1 Surface Impedance of Plane Conductors Consider a semi-infinite, conducting half-space with parameters σ, ε, μ whose surface lies in the x–y plane as shown in Fig. 3.51 [16]. Assume the electric field and associated conduction current density are directed in the z direction. The diffusion equation in terms of this z-directed electric field becomes

$$\frac{d^2 \hat{E}_z}{dx^2} = j\omega\mu\sigma \hat{E}_z \tag{3.181}$$

Similar equations govern the magnetic field, $\hat{H}_y$, and the current density, $\hat{J}_z$. The solutions are

$$\hat{E}_z = \hat{E}_o e^{-x/\delta} e^{-jx/\delta} \tag{3.182a}$$

$$\hat{H}_y = \hat{H}_o e^{-x/\delta} e^{-jx/\delta} \tag{3.182b}$$

$$\hat{J}_z = \hat{J}_o e^{-x/\delta} e^{-jx/\delta} \tag{3.182c}$$

where the familiar *skin depth* is

$$\delta = \frac{1}{\sqrt{\pi f \mu \sigma}} \tag{3.183}$$

and $\hat{E}_o$, $\hat{H}_o$, $\hat{J}_o$ are the appropriate quantities at the surface. This result shows that the fields and current density decay rapidly in the conductor and are essentially confined to layers at the surface of thickness equal to a few skin depths.

The *surface impedance* can be defined as the ratio of the z-directed electric field at the surface and the total current density:

$$\hat{Z}_s = \frac{\hat{E}_o}{\hat{J}_T} \tag{3.184}$$

The total current in the conductor can be obtained by integrating the current density given in (3.182c) throughout the conductor:

$$\hat{J}_T = \int_0^\infty \hat{J}_z \, dx \tag{3.185}$$

$$= \frac{\hat{J}_o \delta}{(1+j)}$$

Substituting into (3.184) gives ($\hat{J}_o = \sigma \hat{E}_o$)

$$\hat{Z}_s = R_s + j\omega L_i \tag{3.186}$$

where

$$R_s = \frac{1}{\sigma \delta} = \sqrt{\frac{\pi f \mu}{\sigma}} \ \Omega/\text{square} \tag{3.187a}$$

$$\omega L_i = R_s \tag{3.187b}$$

This surface impedance is the impedance of an area of the surface of unit width and unit length so that we use the term ohms/square. The term R_s is referred to as the surface resistance, and the term L_i is referred to as the internal inductance. Observe that the surface resistance *increases* as $\sqrt{f}$, whereas the internal inductance *decreases* as $\sqrt{f}$ so that the internal inductive reactance *increases* as $\sqrt{f}$. Observe also that the surface resistance in (3.187a) could have been more easily calculated by assuming the current density to be *constant* in a thickness equal to one skin depth of the surface and zero elsewhere.

Equivalently, the surface impedance can be written as

$$\hat{Z}_s = \sqrt{\frac{j\omega\mu}{\sigma}} \tag{3.188}$$

Essentially we could have obtained the same result from the *intrinsic impedance* of the conductor [A.1]:

$$\hat{\eta} = \sqrt{\frac{j\omega\mu}{\sigma + j\omega\varepsilon}} \tag{3.189}$$

by observing that within the conductor the conduction current dominates the displacement current, i.e., $\sigma \gg \omega\varepsilon$.

3.6.2.2 Resistance and Internal Inductance of Wires Next we consider the *resistance* and *internal inductance* of circular cylindrical conductors (wires). The resistance and internal inductance are again due to the wire conductance being finite. In the case of perfect conductors, the currents flow on the surfaces of the conductors. Resistance and internal inductance result from the current and magnetic flux internal to the imperfect conductors in a fashion similar to the case of the surface impedance of a plane conductor and can be computed in a straightforward fashion if we know the current distribution over the wire cross section. The internal inductance results from magnetic flux internal to the conductor that links the current, whereas the external inductance results from the magnetic flux that is external to the conductors that penetrates the area between the conductor and the reference or other conductors as discussed previously.

The determination of these parameters for wires is very straightforward *if we assume the current is symmetric about the axis of the wire* [16, 22]. At dc the current is uniformly distributed over the cross section, whereas at higher frequencies the current crowds to the surface, being concentrated in annuli of thickness of the order of a skin depth. This observation leads to a useful equivalent circuit representing this skin effect which attempts to mimic this phenomenon [23]. Essentially this assumption of current symmetry about the wire axis means that we assume there are no nearby currents close enough to upset this symmetry (proximity effect) [24]. Neighboring conductors also affect this current distribution for conductors of rectangular cross section [25]. Determination of these parameters when other currents are close enough to upset this symmetry is considerably more difficult, and for typical wire radii and spacings the symmetrical current distribution assumption is adequate. For example, reference [16] gives the exact per-unit-length *high-frequency* resistance for a two-wire line in a homogeneous medium consisting of two identical wires

of radii r_w separated by s as

$$r = \frac{2R_s}{2\pi r_w}\left[\frac{\frac{s}{2r_w}}{\sqrt{\left(\frac{s}{2r_w}\right)^2 - 1}}\right] \Omega/\text{m}$$

where

$$R_s = \frac{1}{\sigma\delta} = \sqrt{\frac{\pi f\mu}{\sigma}}$$

is the surface resistance of the conductor. For $s = 4r_w$ such that one wire exactly fits between the two wires the resistance is only 15% higher than that assuming a uniform current distribution.

Internal to the conductor, the conduction current dominates the displacement current so that the diffusion equation again describes the conduction current distribution internal to the wire. Let us assume that this current density is z directed (along the wire axis) and is symmetric about the axis of the wire and write the diffusion equation in cylindrical coordinates. We orient the wire about the z axis of a cylindrical coordinate system. Because of the assumed symmetry, the current density is independent of z and ϕ but is a function of the radius, r, from the wire axis so that the diffusion equation reduces to [A.1]

$$\frac{d^2\hat{J}_z}{dr^2} + \frac{1}{r}\frac{d\hat{J}_z}{dr} + k^2\hat{J}_z = 0 \tag{3.190}$$

where

$$k^2 = -j\omega\mu\sigma \tag{3.191}$$

$$= -j\frac{2}{\delta^2}$$

The solution to this equation is [A.1, 16, 22]

$$\hat{J}_z = \hat{J}_o \frac{\text{ber}(\sqrt{2}r/\delta) + j\,\text{bei}(\sqrt{2}r/\delta)}{\text{ber}(\sqrt{2}r_w/\delta) + j\,\text{bei}(\sqrt{2}r_w/\delta)} \tag{3.192}$$

where ber(x) and bei(x) are the real and imaginary parts, respectively, of the Bessel function of the first kind of a complex argument [8, 16, 21]. The term $\hat{J}_o$ is the current density at the outer radius of the wire, $r = r_w$.

It now remains to determine the total internal impedance (per unit length) of the wire. The total current in the wire can be found by integrating Ampere's law around the wire surface (assuming that the displacement current within the wire is much less than the conduction current):

$$\hat{I} = \oint \vec{\hat{H}}\cdot d\vec{l} \tag{3.193}$$

$$= 2\pi r_w \hat{H}_\phi|_{r=r_w}$$

The magnetic field can be obtained from Faraday's law multiplied by the wire

conductivity:

$$\nabla \times \vec{J} = -j\omega\mu\sigma\vec{H} \tag{3.194}$$

Substituting the result for curl in cylindrical coordinates [A.1] and recalling that the current density is z directed and dependent only on r and the magnetic field is ϕ directed gives

$$\frac{d\hat{J}_z}{dr} = j\omega\mu\sigma\hat{H}_\phi \tag{3.195}$$

Substituting this into (3.193) and using (3.192) gives the total current in terms of the current at the wire surface. The per-unit-length internal impedance becomes

$$\begin{aligned} \hat{z}_{\text{int}} &= \frac{\hat{E}_z|_{r=r_w}}{\hat{I}} \qquad (3.196a) \\ &= \frac{j\omega\mu\sigma}{2\pi r_w\sigma}\frac{\hat{J}_z|_{r=r_w}}{\left.\dfrac{d\hat{J}_z}{dr}\right|_{r=r_w}} \\ &= \frac{1}{\sqrt{2}\pi r_w\sigma\delta}\left[\frac{\text{ber}(q) + j\,\text{bei}(q)}{\text{bei}'(q) - j\,\text{ber}'(q)}\right]\Omega/\text{m} \end{aligned}$$

where

$$\text{ber}'(q) = \frac{d}{dq}\text{ber}(q)$$

$$\text{bei}'(q) = \frac{d}{dq}\text{bei}(q)$$

and

$$q = \sqrt{2}\,\frac{r_w}{\delta} \tag{3.196b}$$

Writing this total internal impedance in terms of its real and imaginary parts as

$$\hat{z}_{\text{int}} = r + j\omega l_i \tag{3.197}$$

gives the conductor resistance and internal inductance as

$$\frac{r}{r_{dc}} = \frac{q}{2}\left[\frac{\text{ber}(q)\text{bei}'(q) - \text{bei}(q)\text{ber}'(q)}{(\text{bei}'(q))^2 + (\text{ber}'(q))^2}\right] \tag{3.198}$$

$$\frac{l_i}{l_{i,dc}} = \frac{4}{q}\left[\frac{\text{bei}(q)\text{bei}'(q) + \text{ber}(q)\text{ber}'(q)}{(\text{bei}'(q))^2 + (\text{ber}'(q))^2}\right] \tag{3.199}$$

where

$$r_{dc} = \frac{1}{\sigma\pi r_w^2}\ \Omega/\text{m} \tag{3.200}$$

$$l_{i,dc} = \frac{\mu_o}{8\pi} = 0.5 \times 10^{-7}\ \text{H/m} \tag{3.201}$$

are the dc per-unit-length resistance and internal inductance, respectively, of the wire [A.1].

Although the results in (3.198) and (3.199) are exact assuming a current distribution that is *symmetric* about the wire axis, they are somewhat complicated. Reasonable simplifications can be obtained depending on whether the frequency is such that the wire radius is greater than or less than a skin depth. Figure 3.52 shows the ratio of the per-unit-length resistance and the dc resistance of (3.198) plotted as a function of the ratio of the wire radius and a skin depth, r_w/δ. Observe that the transition to $\sqrt{f}$ frequency dependence commences around the point where the wire radius is two skin depths, $r_w = 2\delta$. Similarly, Fig. 3.53 shows the ratio of the per-unit-length internal inductance and the dc internal inductance of (3.199) plotted as a function of the ratio of wire radius to skin depth. The transition to $\sqrt{f}$ frequency dependence commences at the same point as for the resistance. Consequently, the exact results can be approximated by

$$\left.\begin{aligned} r &= \frac{1}{\sigma\pi r_w^2}\ \Omega/\text{m} \\ l_i &= \frac{\mu_o}{8\pi} = 0.5 \times 10^{-7}\ \text{H/m} \end{aligned}\right\} r_w < 2\delta \tag{3.202a}$$

$$\left.\begin{aligned} r &= \frac{1}{2\pi r_w \sigma\delta} = \frac{1}{2r_w}\sqrt{\frac{\mu}{\pi\sigma}}\sqrt{f}\ \Omega/\text{m} \\ l_i &= \frac{1}{4\pi r_w}\sqrt{\frac{\mu}{\pi\sigma}}\frac{1}{\sqrt{f}}\ \text{H/m} \end{aligned}\right\} r_w > 2\delta \tag{3.202b}$$

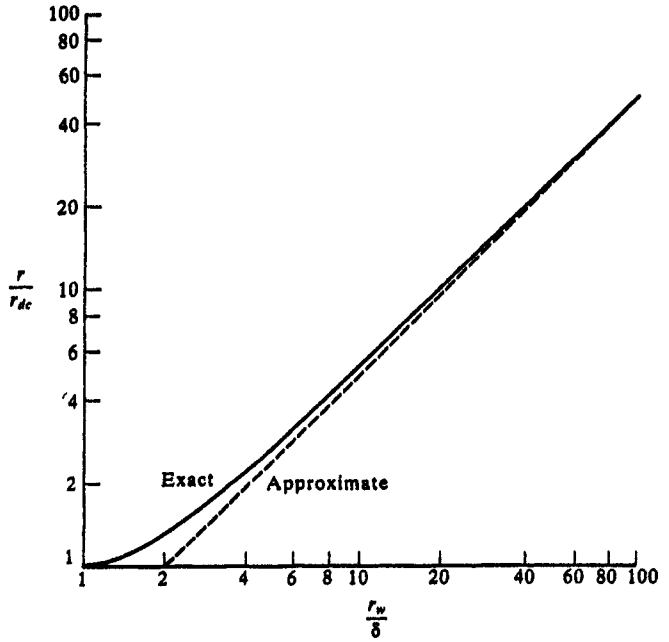

FIGURE 3.52 Frequency dependence of the per-unit-length resistance of a wire as a function of the ratio of wire radius to skin depth.

Observe that the *low-frequency resistance* for $r_w < 2\delta$ in (3.202a) could have been computed by assuming the current is uniformly distributed over the cross section as illustrated in Fig. 3.54(a); this is the case at dc. Similarly, the *high-frequency resistance* for $r_w > 2\delta$ in (3.202b) could have been computed by assuming the current is uniformly distributed over an annulus at the wire surface of thickness equal to one skin depth as illustrated in Fig. 3.54(b); this satisfies our intuition based on the plane conductor case. Considering the complexity of the exact results we will use these approximations in our future work.

3.6.2.3 Internal Impedance of Rectangular Cross Section Conductors Unlike wires, analytical solutions for the resistance and internal inductance of conductors of rectangular cross section are complicated by the fact that we do not know the current distribution over the cross section. The current distribution over the cross section of a rectangular conductor tends to be concentrated at the corners when the skin effect is well developed. Early works consisted of measured results for the skin effect [26–27]. Wheeler developed a simple "incremental inductance rule" for computing the high-frequency impedance when the skin effect is well developed [28]. This rule continues to be used extensively. The direct solution for the resistance and internal inductance of conductors of rectangular cross section can be obtained using a variety of

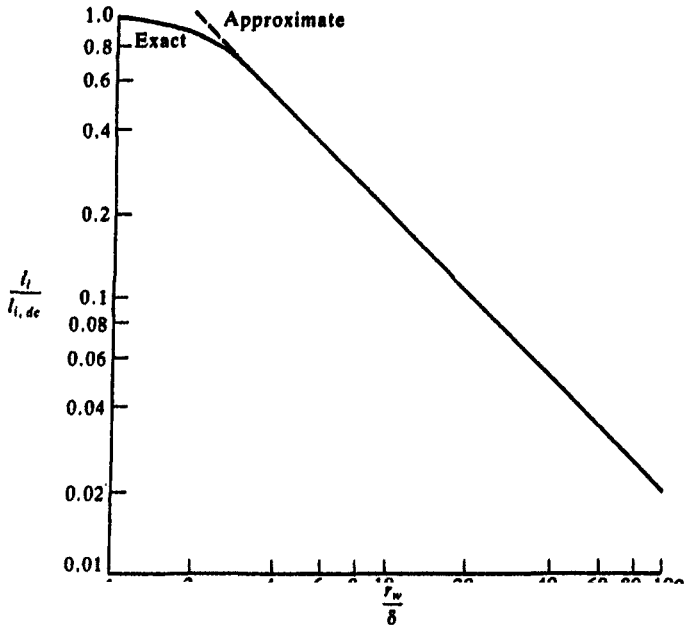

FIGURE 3.53 Frequency dependence of the per-unit-length internal inductance of a wire as a function of the ratio of wire radius to skin depth.

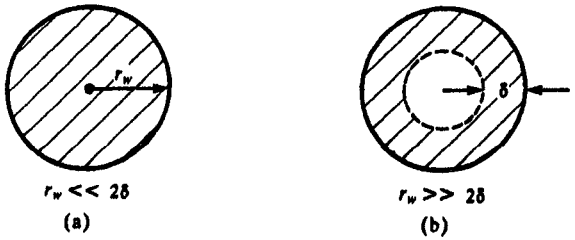

FIGURE 3.54 Illustration of the cross-sectional current distribution of a wire for (a) low frequencies and (b) high frequencies.

methods for solving the diffusion equation in the two-dimensional transverse plane for infinitely long conductors [28–37]. For example, finite element methods are implemented in several commercial packages. Another common and less direct method is the perturbation technique [18].

A particularly simple (conceptually) numerical method for determining these quantities is described in [38]. This technique determines the resistance and internal inductance for conductors of actual lengths and so includes end effects, whereas the two-dimensional methods do not. It uses the concepts of partial

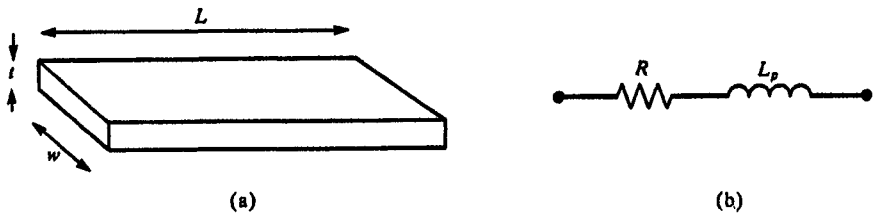

FIGURE 3.55 Circuit representation of a rectangular bar.

inductance [A.3, 39–41]. Figure 3.55(a) shows a bar of length L, width w, and thickness t. If we assume the current to be uniformly distributed over the cross section the total bar resistance can be easily determined as

$$R = \frac{L}{\sigma w t}\ \Omega \tag{3.203}$$

The partial inductance, L_p, can be similarly determined for uniform current distribution over the cross section [39–41]. This notion can be extended to bars that have nonuniform current distributions over their cross section by dividing the bar into N subbars of rectangular cross section over which we assume the current to be uniformly distributed but whose level is unknown as illustrated in Fig. 3.56(a). This essentially approximates the actual current distribution over the cross section as a step. The voltage across each subbar is

$$\hat{E} = R_i \hat{I}_i + j\omega L_{pi} \hat{I}_i + j\omega \sum_{\substack{k=1 \\ k \neq i}}^{N} (L_{pik} \hat{I}_k) \tag{3.204}$$

where L_{pik} is the mutual partial inductance between the i-th and k-th subbars which contains the relative locations of the subbars. Formulas for these mutual partial inductances between conductors of rectangular cross section having uniformly distributed currents over their cross section are also available in [39–41]. Arranging (3.204) for all subbars gives

$$\begin{bmatrix} \hat{E} \\ \hat{E} \\ \vdots \\ \hat{E} \end{bmatrix} = \begin{bmatrix} (R_1 + j\omega L_{p1}) & j\omega L_{p12} & \cdots & j\omega L_{p1N} \\ j\omega L_{p12} & (R_2 + j\omega L_{p2}) & \ddots & j\omega L_{p2N} \\ \vdots & \vdots & \ddots & \vdots \\ j\omega L_{p1N} & j\omega L_{p2N} & \cdots & (R_N + j\omega L_{pN}) \end{bmatrix} \begin{bmatrix} \hat{I}_1 \\ \hat{I}_2 \\ \vdots \\ \hat{I}_N \end{bmatrix} \tag{3.205a}$$

or

$$\hat{\mathbf{E}} = \hat{\mathbf{Z}}\hat{\mathbf{I}} \tag{3.205b}$$

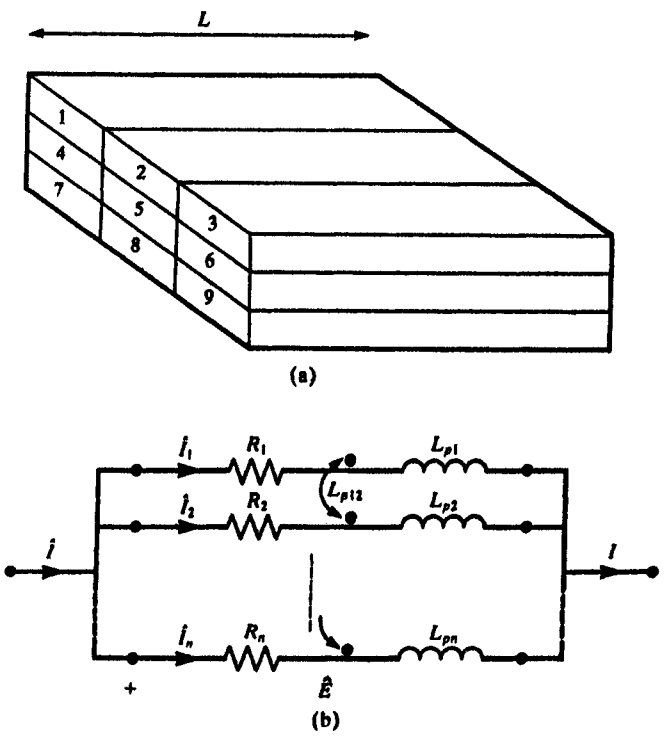

FIGURE 3.56 Representation of (a) a rectangular bar having a nonuniform current distribution over the cross section in terms of subbars having constant current distribution and (b) the resulting circuit model.

for N subbars. The sum of the subbar currents equals the total current for the bar and the voltages across all subbars are equal to the voltage across the bar as illustrated in Fig. 3.56. These constraints can be imposed to give the total resistance and partial inductance of the overall bar by inverting $\hat{\mathbf{Z}}$ in (3.205) to yield $\hat{\mathbf{I}} = \hat{\mathbf{Z}}^{-1}\hat{\mathbf{E}}$. The first constraint is imposed by summing the entries in the rows, and the second constant is imposed by summing the entries in the columns of that result to give the effective parameters of the complete bar including skin effect as

$$\hat{z} = \sum_{i=1}^{N}\sum_{j=1}^{N}[\hat{\mathbf{Z}}^{-1}]_{ij} \tag{3.206}$$

$$= R(f) + j\omega(L_i(f) + L_e)$$

The resulting composite resistance, $R(f)$, includes the effect of nonuniform current distribution over the bar cross section. The imaginary part includes the

internal inductance, $L_i(f)$, (due to flux internal to the conductor) which is also frequency dependent. This result includes the effect of flux external to the conductor through L_e. The internal inductance decreases as $\sqrt{f}$ due to less internal flux linkages for increasing frequency as the current crowds to the surface of the bar and is typically dominated by the external inductance.

Proximity effects of nearby conductors on these skin effect parameters can also be included in the method. Consider a MTL consisting of $n + 1$ conductors of rectangular cross section with the reference conductor numbered as the zeroth conductor. Each conductor is subsectioned into N_i subbars for $i = 0, 1, \ldots, n$. Writing (3.205) for the system gives $N_T = \sum_{i=0}^{n+1} N_i$ equations:

$$\begin{bmatrix} \hat{\mathbf{E}}_0 \\ \hat{\mathbf{E}}_1 \\ \vdots \\ \hat{\mathbf{E}}_n \end{bmatrix} = \begin{bmatrix} \hat{\mathbf{Z}}_0 & j\omega\mathbf{M}_{01} & \cdots & j\omega\mathbf{M}_{0n} \\ j\omega\mathbf{M}_{01} & \hat{\mathbf{Z}}_1 & \ddots & j\omega\mathbf{M}_{1n} \\ \vdots & \ddots & \ddots & \vdots \\ j\omega\mathbf{M}_{0n} & j\omega\mathbf{M}_{1n} & \cdots & \hat{\mathbf{Z}}_n \end{bmatrix} \begin{bmatrix} \hat{\mathbf{I}}_0 \\ \hat{\mathbf{I}}_1 \\ \vdots \\ \hat{\mathbf{I}}_n \end{bmatrix} \tag{3.207}$$

Inverting this matrix gives

$$\begin{bmatrix} \hat{\mathbf{I}}_0 \\ \hat{\mathbf{I}}_1 \\ \vdots \\ \hat{\mathbf{I}}_n \end{bmatrix} = \begin{bmatrix} \hat{\mathbf{Y}}_{00} & \hat{\mathbf{Y}}_{01} & \cdots & \hat{\mathbf{Y}}_{0n} \\ \hat{\mathbf{Y}}_{01} & \hat{\mathbf{Y}}_{11} & \ddots & \hat{\mathbf{Y}}_{1n} \\ \vdots & \ddots & \ddots & \vdots \\ \hat{\mathbf{Y}}_{0n} & \hat{\mathbf{Y}}_{1n} & \cdots & \hat{\mathbf{Y}}_{nn} \end{bmatrix} \begin{bmatrix} \hat{\mathbf{E}}_0 \\ \hat{\mathbf{E}}_1 \\ \vdots \\ \hat{\mathbf{E}}_n \end{bmatrix} \tag{3.208}$$

First the voltages of each subbar of a bar must be equal. To enforce this condition we sum the entries in the respective columns of the submatrices to yield

$$\begin{bmatrix} \hat{\mathbf{I}}_0 \\ \hat{\mathbf{I}}_1 \\ \vdots \\ \hat{\mathbf{I}} \end{bmatrix} = \begin{bmatrix} \hat{\mathbf{B}}_{00} & \hat{\mathbf{B}}_{01} & \cdots & \hat{\mathbf{B}}_{0n} \\ \hat{\mathbf{B}}_{01} & \hat{\mathbf{B}}_{11} & \ddots & \hat{\mathbf{B}}_{1n} \\ \vdots & \ddots & \ddots & \vdots \\ \hat{\mathbf{B}}_{0n} & \hat{\mathbf{B}}_{1n} & \cdots & \hat{\mathbf{B}}_{nn} \end{bmatrix} \begin{bmatrix} \hat{E}_0 \\ \hat{E}_1 \\ \vdots \\ \hat{E}_n \end{bmatrix} \tag{3.209}$$

where the *vectors* $\hat{\mathbf{B}}_{ij}$ are

$$\hat{\mathbf{B}}_{ij} = \sum_{\text{columns}} \hat{\mathbf{Y}}_{ij} \tag{3.210}$$

The sum of the subbar currents must equal the current of the bar. Implementing

this in (3.209) yields

$$\begin{bmatrix} \hat{I}_0 \\ \hat{I}_1 \\ \vdots \\ \hat{I}_n \end{bmatrix} = \begin{bmatrix} \hat{Y}_{00} & \hat{Y}_{01} & \cdots & \hat{Y}_{0n} \\ \hat{Y}_{01} & \hat{Y}_{11} & \ddots & \hat{Y}_{1n} \\ \vdots & \ddots & \ddots & \vdots \\ \hat{Y}_{0n} & \hat{Y}_{1n} & \cdots & \hat{Y}_{nn} \end{bmatrix} \begin{bmatrix} \hat{E}_0 \\ \hat{E}_1 \\ \vdots \\ \hat{E}_n \end{bmatrix} \tag{3.211}$$

where

$$\hat{Y}_{ij} = \sum_{\text{rows}} \hat{\mathbf{B}}_{ij} \tag{3.212}$$

The sum of the currents of the n conductors must equal that of the reference conductor

$$\hat{I}_0 = -\sum_{k=1}^{n} \hat{I}_k \tag{3.213}$$

in order for the concept of partial inductance to make sense. The difference in the transmission line voltages at the two ends of the line are

$$\Delta \hat{V}_i = \hat{E}_i - \hat{E}_0 \tag{3.214}$$

These concepts are virtually identical to the concepts of the generalized capacitance matrix obtained in Section 3.1.4. Therefore, by adapting the generalized capacitance relations in (3.19), we can obtain

$$\begin{bmatrix} \hat{I}_1 \\ \vdots \\ \hat{I}_n \end{bmatrix} = \begin{bmatrix} \hat{y}_{11} & \cdots & \hat{y}_{1n} \\ \vdots & \ddots & \vdots \\ \hat{y}_{1n} & \cdots & \hat{y}_{nn} \end{bmatrix} \begin{bmatrix} \Delta \hat{V}_1 \\ \vdots \\ \Delta \hat{V}_n \end{bmatrix} \tag{3.215}$$

where

$$\hat{y}_{ij} = \hat{Y}_{ij} - \frac{\left(\sum_{k=0}^{n} \hat{Y}_{ik}\right)\left(\sum_{m=0}^{n} \hat{Y}_{mj}\right)}{\sum \hat{\mathbf{Y}}} \tag{3.216}$$

Inverting this $n \times n$ matrix gives

$$\begin{bmatrix} \Delta \hat{V}_1 \\ \vdots \\ \Delta \hat{V}_n \end{bmatrix} = \begin{bmatrix} \hat{z}_{11} & \cdots & \hat{z}_{1n} \\ \vdots & \ddots & \vdots \\ \hat{z}_{1n} & \cdots & \hat{z}_{nn} \end{bmatrix} \begin{bmatrix} \hat{I}_1 \\ \vdots \\ \hat{I}_n \end{bmatrix} \tag{3.217}$$

Dividing the $\hat{z}_{ij}$ entries by the segment length, L, gives an approximation to

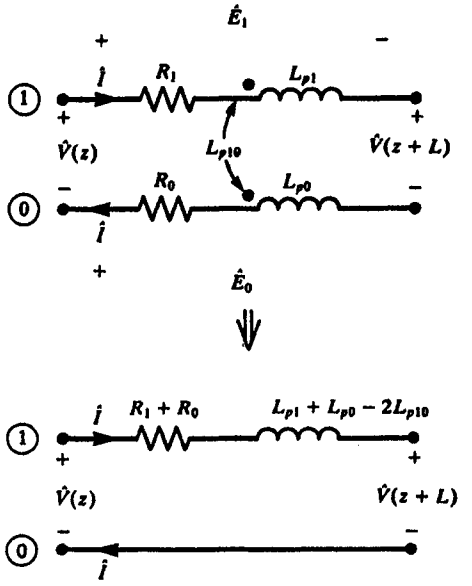

FIGURE 3.57 Reduction of the partial element model to the transmission-line model for a two-conductor line.

the per-unit-length impedance matrix of the line which contains resistance, internal inductance, and external inductance. This process is illustrated for a two-conductor line in Fig. 3.57. The inverse of (3.211) gives the resistances and partial inductances of the two conductors:

$$\begin{bmatrix} \hat{E}_0 \\ \hat{E}_1 \end{bmatrix} = \begin{bmatrix} R_0 + j\omega L_{p0} & j\omega L_{p10} \\ j\omega L_{p10} & R_1 + j\omega L_{p1} \end{bmatrix} \begin{bmatrix} \hat{I}_0 = -\hat{I} \\ \hat{I}_1 = \hat{I} \end{bmatrix} \tag{3.218}$$

where we have used the necessary requirement that the net current at any cross section is zero. Writing the difference of the bar voltages gives

$$\Delta\hat{V} = \hat{E}_1 - \hat{E}_0 = R_1 + R_0 + j\omega(L_{p1} + L_{p0} - 2L_{p10}) \tag{3.219}$$

The reader can verify that this result, derived directly for the special case of a two-conductor line, is equivalent to using the general result in (3.216).

Computations for various bar dimensions are given in [42]. The above method not only models the skin effect over the bar cross sections but also implicitly includes the proximity effect since the mutual partial inductances between each subbar within a bar and between those of the bars of the system are included.

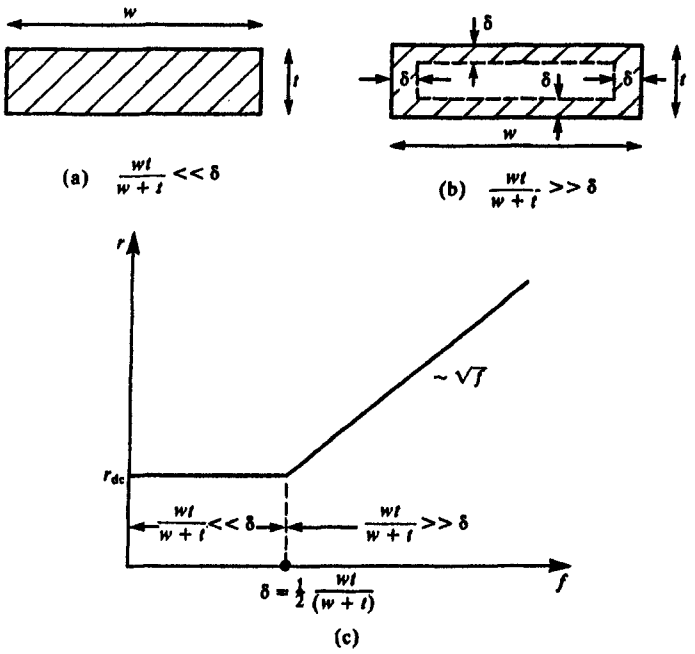

FIGURE 3.58 Illustration of the current distribution over the cross section of a PCB land for low and high frequencies.

The above method is quite accurate if the number of subbars is chosen sufficiently large but it is computationally intensive. A simple method, analogous to that for a round wire, is to approximate the resistance for the two cases where the bar dimensions are much less than or much greater than a skin depth. In the case where the bar dimensions are much less than a skin depth, the current is reasonably approximated as being uniform over the bar cross section as illustrated in Fig. 3.58(a). Thus the low-frequency, dc per-unit-length resistance can be simply calculated as

$$r_{dc} = \frac{1}{\sigma wt} \ \Omega/\text{m} \tag{3.220}$$

For higher frequencies where the bar dimensions are much greater than a skin depth, i.e., the skin effect is well developed, we assume that the current is uniformly distributed over strips of thickness δ and zero elsewhere as illustrated in Fig. 3.58(b). As will be shown subsequently, the current peaks at the corners of the bar when the skin effect is well developed but this effect is ignored here.

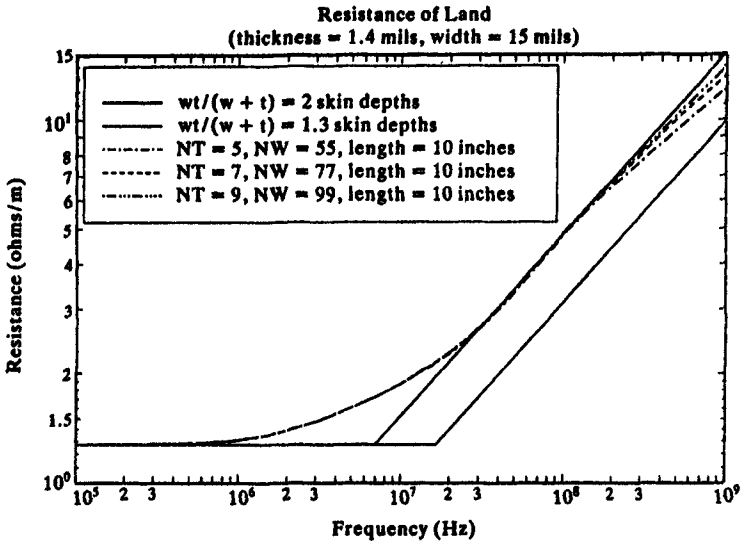

FIGURE 3.59 Results of the computation of the per-unit-length resistance of a land via the method of subbars. Thickness = 1.4 mils, width = 15 mils.

This gives the high-frequency per-unit-length resistance as

$$r_{hf} = \frac{1}{\sigma(2\delta t + 2\delta w)} = \frac{1}{2\sigma\delta(w + t)} \tag{3.221}$$

which increases as $\sqrt{f}$. This high-frequency result is less than the actual value because of the peaking of the current at the bar corners at high frequencies. The two regions join at

$$\delta = \frac{1}{2}\frac{wt}{(w + t)} \cong \frac{t}{2} \qquad w \gg t \tag{3.222}$$

as shown in Fig. 3.58(c). For bars having high aspect ratios, $w \gg t$, the two curves join where the thickness (the smaller dimension) equals two skin depths, which satisfies our intuition. Results given in [43, 44] indicate the sufficiency of the above approximation. Figure 3.59 illustrates the comparison of this approximation to the method of subbars described previously for various divisions of the bar (w/NW, t/NT). The resistance of the bar is the real part of $\hat{z}$ computed as in (3.206). The bar is typical of a "land" on the surface of a

printed circuit board and has $t = 1.4$ mils and $w = 15$ mils. The results were computed for bar lengths of 1 inch and 10 inches, and the per-unit-length resistance obtained by dividing the total resistance by the bar length was virtually identical for the two lengths. The break frequency in (3.222) occurs around 16.514 MHz where the average dimension $wt/(w + t)$ in (3.222) is two skin depths. The subbar method indicates that the true resistance in the high-frequency region is some 50% higher than that predicted by the approximate method but nevertheless varies as $\sqrt{f}$. This error is evidently due to the omission of the peaking of the current at the corners in the approximation. The approximate method could be modified by using a lower break frequency. Choosing the break frequency where the average dimension is equal to only 1.3δ gives a result that exactly matches the high-frequency result. However this better approximation cannot be assumed to hold for other dimensions or for the case where nearby lands alter the current distribution so that the break frequency will be chosen as in (3.222). Considering the considerable computational effort involved in a numerical solution (a large number of simultaneous equations (3.205) for one bar or (3.207) for several bars must be inverted *at each frequency of interest*) we will choose to use the simple approximate method in computing the skin-effect per-unit-length resistances for rectangular-cross-section lands in our future computed results. Figure 3.60 shows the normalized current distribution over the land cross section computed for a land of total length 10 inches, using nine divisions along the thickness, and ninety-nine divisions along the width. These plots confirm that for frequencies where the land dimensions are much less than a skin depth, the current is uniformly distributed over the cross section; whereas for frequencies where the skin effect is well developed, the current distribution peaks at the land corners.

It is reasonable to assume that the bar internal inductance similarly varies as the dc value below the same break frequency and decreases as $\sqrt{f}$ above this. So a simple approximate method for its determination will similarly suffice. For typical line dimensions this is dominated by the external inductance due to magnetic flux external to the wires computed for perfect conductors. Again, the inductive reactance due to the high-frequency internal inductance varies as the square root of frequency, $\omega l_i \approx \sqrt{f}$, yet the inductive reactance due to the external inductance varies directly with frequency as $\omega l_e \approx f$.

3.6.2.4 Approximate Representation of Conductor Internal Impedances in the Frequency Domain The total per-unit-length internal impedance of a conductor in the frequency domain has a real part due to the conductor resistance and an imaginary part due to the internal inductive reactance:

$$\mathcal{Z}_i(\omega) = r_i(\omega) + j\omega l_i(\omega) \tag{3.223}$$

We will assume that the high-frequency resistance varies as $\sqrt{f}$ for $f > f_o$ and

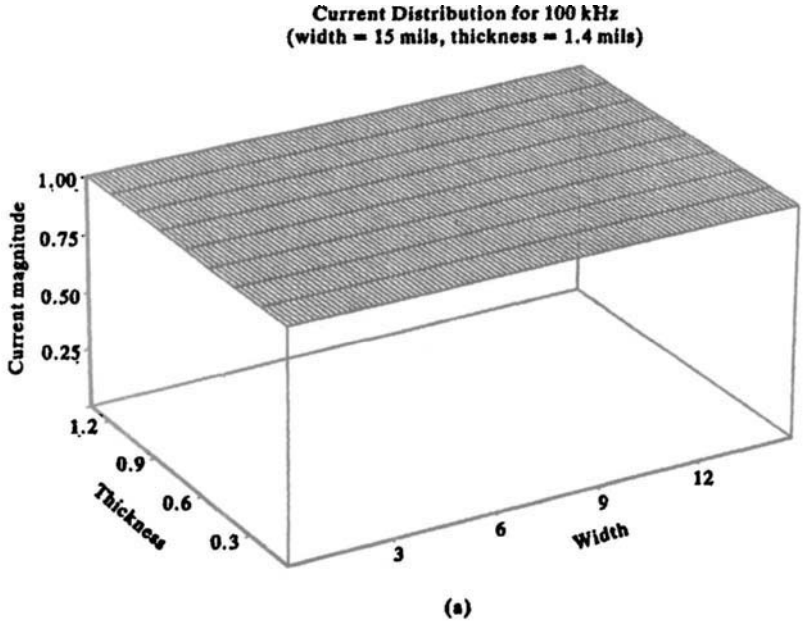

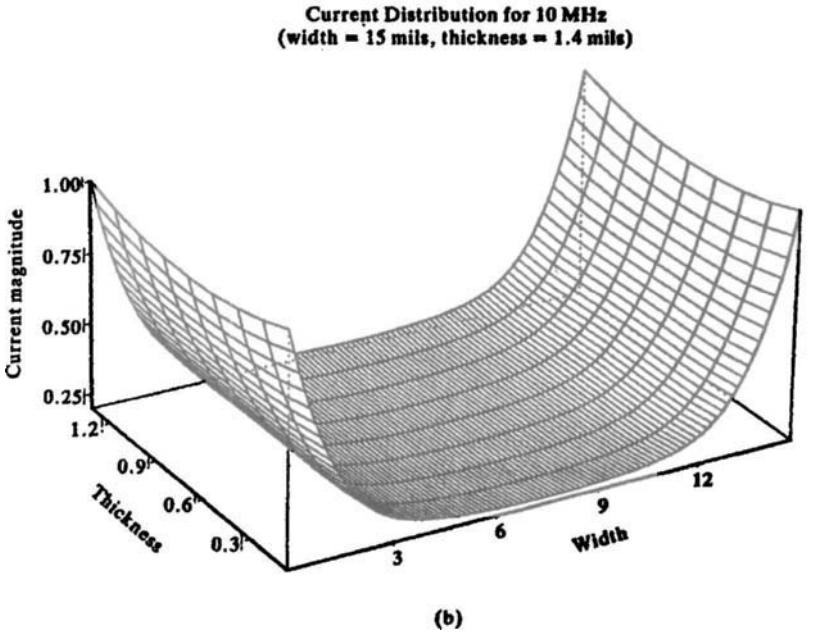

FIGURE 3.60 Illustration of the cross-sectional current distribution of a PCB land for (a) 100 kHz, (b) 10 MHz.

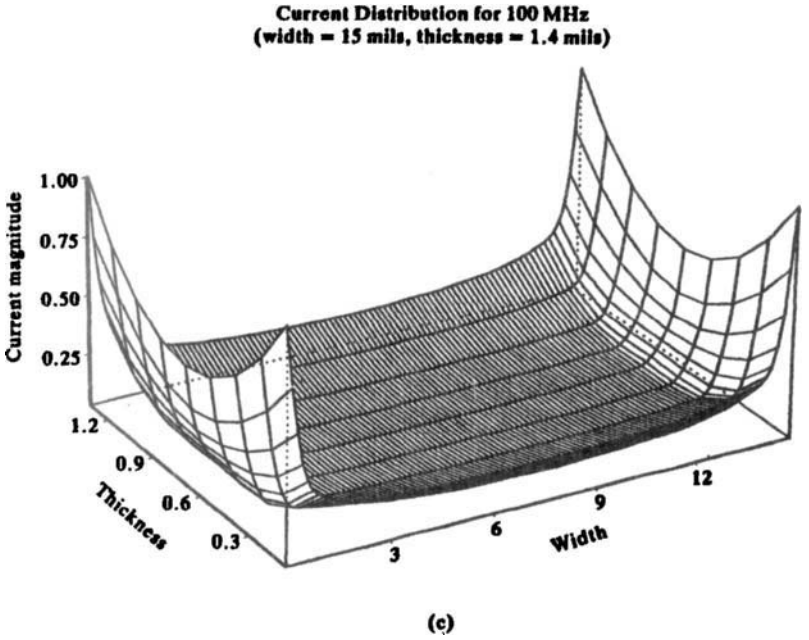

(c)

FIGURE 3.60 *Continued.* (c) 100 MHz. Thickness = 1.4 mils, width = 15 mils.

is constant at the dc value below this:

$$r_i = \begin{cases} r_{dc} & f \le f_o \\ r_{dc}\sqrt{f/f_o} & f \ge f_o \end{cases} \tag{3.224}$$

Let us also assume that the high-frequency internal inductive reactance equals the high-frequency resistance, $r_{i,hf} = \omega l_{i,hf}$, and also transitions to the dc internal inductive reactance, $\omega l_{i,dc}$, at f_o. Therefore the dc internal inductance can be written as $l_{i,dc} = r_{dc}/\omega_o$. The equality of high-frequency resistance and internal inductive reactance is demonstrated for all conductor cross sections by Wheeler's "incremental inductance rule" [28]. Also we showed previously that the resistance and internal inductance of solid wires transition at precisely the same frequency. With these approximations the conductor internal impedance can be approximated as

$$\hat{z}_i(\omega) = \begin{cases} r_{dc}(1 + jf/f_o) & f \le f_o \\ r_{dc}\sqrt{f/f_o}(1 + j) & f \ge f_o \end{cases} \tag{3.225}$$

Thus in this approximation one need only know the dc per-unit-length resistance and the frequency that it transitions to the high-frequency $\sqrt{f}$

frequency dependence due to the skin effect. Of course this approximation will be in error at the transition frequency (see Figs. 3.52 and 3.53 for wires) but the required input data for the frequency-domain computer programs that use these will be minimized.

Representation of this frequency dependence of the conductor internal impedances in the time domain will be investigated in Chapter 5 when we seek to determine the time-domain solution of the MTL equations. We will represent the conductor internal impedances as

$$z_i(s) = A + B\sqrt{s} \tag{3.226}$$

where the Laplace transform variable is denoted as s. That this is a reasonable representation of the conductor impedances can be demonstrated by substituting $s \Leftrightarrow j\omega$ giving

$$\begin{aligned} z_i(\omega) &= A + B\sqrt{j\omega} \\ &= A + B\sqrt{\pi}\sqrt{f}(1+j) \end{aligned} \tag{3.227}$$

Thus we may interpret, in this approximation,

$$A = r_{dc} \tag{3.228a}$$

$$\begin{aligned} B\sqrt{\pi}\sqrt{f}(1+j) &= r_{hf} + j\omega l_{i,hf} \\ &= r_{dc}\sqrt{\frac{f}{f_o}}(1+j) \end{aligned} \tag{3.228b}$$

REFERENCES

[1] W.B. Boast, *Vector Fields*, Harper & Row, N.Y, 1964.

[2] E. Weber, *Electromagnetic Fields*, Vol. I, John Wiley, NY, 1950.

[3] W.R. Smythe, *Static and Dynamic Electricity*, 3d ed., McGraw-Hill, NY, 1968.

[4] A.T. Adams, *Electromagnetics for Engineers*, Ronald Press, NY, 1971.

[5] R.F. Harrington, *Field Computation by Moment Methods*, Macmillan, NY, 1968.

[6] M.N.O. Sadiku, *Numerical Techniques in Electromagnetics*, CRC Press, Boca Raton, FL, 1992.

[7] W.T. Weeks, "Calculation of Coefficients of Capacitance of Multiconductor Transmission Lines in the Presence of a Dielectric Interface," *IEEE Trans. on Microwave Theory and Techniques*, MTT-18, 35–43 (1970).

[8] H.B. Dwight, *Tables of Integrals and Other Mathematical Data*, Macmillan, NY, 4th ed., 1961.

[9] M. Javid and P.M. Brown, *Field Analysis and Electromagnetics*, McGraw-Hill, NY, 1963.

[10] P.P. Sylvester and R.L. Ferrari, *Finite Elements for Electrical Engineers*, 2d ed., Cambridge University Press, NY, 1990.

[11] S. Frankel, *Multiconductor Transmission Line Analysis*, Artech House, Dedham, MA, 1977.

[12] K.C. Gupta, R. Garg, and I.J. Bahl, *Microstrip Lines and Slotlines*, Artech House, Dedham, MA, 1979.

[13] R.E. Collin, *Field Theory of Guided Waves*, 2d ed., IEEE Press, NY, 1991.

[14] H.A. Wheeler, "Transmission-Line Properties of Parallel Strips Separated by a Dielectric Sheet," *IEEE Trans. on Microwave Theory and Techniques*, **MTT-13**, 172–185 (1965).

[15] E. Yamashita, "Variational Methods for the Analysis of Microstrip-Like Transmission Lines," *IEEE Trans. on Microwave Theory and Techniques*, **MTT-16**, 529–535 (1968).

[16] S. Ramo, J.R. Whinnery, and T. Van Duzer, *Fields and Waves in Communication Electronics*, 2d ed., John Wiley, NY, 1984.

[17] A.R. von Hippel, *Dielectric Materials and Applications*, MIT Press and Wiley, NY, 1954.

[18] R.F. Harrington and C. Wei, "Losses in Multiconductor Transmission Lines in Multilayered Dielectric Media," *IEEE Trans. on Microwave Theory and Techniques*, **MTT-32**, 705–710 (1984).

[19] J. Venkataraman, et al., "Analysis of Arbitrarily Oriented Microstrip Transmission Lines in Arbitrarily Shaped Dielectric Media over a Finite Ground Plane," *IEEE Trans. on Microwave Theory and Techniques*, **MTT-33**, 952–959 (1985).

[20] M.V. Schneider, "Dielectric Losses in Integrated Circuits," *Bell System Technical Journal*, **48**, 2325–2332 (1969).

[21] R.E. Matick, *Transmission Lines for Digital and Communication Networks*, McGraw-Hill, NY, 1969.

[22] W.C. Johnson, *Transmission Lines and Networks*, McGraw-Hill, NY, 1950.

[23] C. Yen, Z. Fazarinc and R.L. Wheeler, "Time-Domain Skin-Effect Model for Transient Analysis of Lossy Transmission Lines," *Proc. IEEE*, **70**, 750–757 (1982).

[24] V. Belevitch, "Theory of the Proximity Effect in Multiwire Cables," *Philips Research Reports*, **32**, Part I, 16-43 (1977); **32**, Part II, 96–177 (1977).

[25] M.E. Hellman and I. Palocz, "The Effect of Neighboring Conductors on the Currents and Fields in Plane Parallel Transmission Lines," *IEEE Trans. on Microwave Theory and Techniques*, **MTT-17**, 254–258 (1969).

[26] J.D. Cockcroft, "Skin Effect in Rectangular Conductors at High Frequencies," *Proc. Roy. Soc.*, **122**, 533–542 (1929).

[27] S.J. Haefner, "Alternating Current Resistance of Rectangular Conductors," *Proc. IRE*, **25**, 434–447 (1937).

[28] H.A. Wheeler, "Formulas for the Skin-Effect," *Proc. IRE*, **30**, 412–424 (1942).

[29] P. Silvester, "Modal Theory of Skin Effect in Flat Conductors," *Proc. IEEE*, **54**, 1147–1151 (1966).

[30] P. Silvester, "The Accurate Calculation of Skin Effect of Complicated Shape," *IEEE Trans. on Power Apparatus and Systems*, **PAS-87**, 735–742 (1968).

[31] M.J. Tsuk and J.A. Kong, "A Hybrid Method for the Calculation of the Resistance and Inductance of Transmission Lines with Arbitrary Cross Sections," *IEEE Trans. on Microwave Theory and Techniques*, **MTT-39**, 1338–1347 (1991).

[32] F. Olyslager, N. Fache, and D. De Zutter, "A Fast and Accurate Line Parameter Calculation of General Multiconductor Transmission Lines in Multilayered Media," *IEEE Trans. on Microwave Theory and Techniques*, **MTT-39**, 901–909 (1991).

[33] P. Waldow and I. Wolff, "The Skin-Effect at High Frequencies," *IEEE Trans. on Microwave Theory and Techniques*, **MTT-33**, 1076–1081 (1985).

[34] H. Lee and T. Itoh, "Phenomenological Loss Equivalence Method for Planar Quasi-TEM Transmission Lines with a Thin Normal Conductor or Superconductor," *IEEE Trans. on Microwave Theory and Techniques*, **37**, 1904–1909 (1989).

[35] G.I. Costache, "Finite Element Method Applied to Skin-Effect Problems in Strip Transmission Lines," *IEEE Trans. on Microwave Theory and Techniques*, **35**, 1009–1013 (1987).

[36] T. Itoh (ed.), *Planar Transmission Line Structures*, IEEE Press, NY, 1987.

[37] E.L. Barsotti, E.F. Kuester, and J.M. Dunn," "A Simple Method to Account for Edge Shape in the Conductor Loss in Microstrip," *IEEE Trans. on Microwave Theory and Techniques*, **MTT-39**, 98–105 (1991).

[38] W.T. Weeks, L.L. Wu, M.F. McAlister, and A. Singh, "Resistive and Inductive Skin Effect in Rectangular Conductors," *IBM J. Research and Development*, **23**, 652–660 (1979).

[39] A.E. Ruehli, "Inductance Calculations in a Complex Integrated Circuit Environment," *IBM J. Research and Development*, **16**, 470–481 (1972).

[40] F.W. Grover, *Inductance Calculations*, Dover Publications, NY, 1946.

[41] C. Hoer and C. Love, "Exact Inductance Equations for Rectangular Conductors with Applications to More Complicated Geometries," *J. Res. Nat. Bureau of Standards-C. Eng. Instrum.*, **69C**, 127–137 (1965).

[42] A.W. Barr, "Calculation of Frequency-Dependent Impedance for Conductors of Rectangular Cross Section," *AMP J. Technology*, **1**, 91–100 (1991).

[43] T.V. Dinh, B. Cabon, and J. Chilo, "New Skin-Effect Circuit," *Electronics Letters*, **26**, 1582–1584 (1990).

[44] A. Deutsch et al., "High-Speed Signal Propagation on Lossy Transmission Lines," *IBM J. Research and Development*, **34**, 601–615 (1990).

PROBLEMS

3.1 A coaxial cable with a symmetrically inhomogeneous interior medium is shown in Fig. P3.1. Determine the per-unit-length capacitance, inductance, and conductance for this transmission line.

3.2 Consider a pair of parallel #28 gauge (r_w = 7.5 mils, 1 mil = 0.001 inch) wires separated a distance of 50 mils as in a ribbon cable. Determine the per-unit-length capacitance, c, and inductance, l, for this transmission

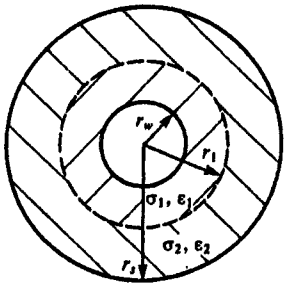

FIGURE P3.1

line if the surrounding medium is free space. The wires are stranded with seven strands of #36 gauge ($r_w = 2.5$ mils) solid wires. Considering these seven wire strands to be connected electrically in parallel, compute the total wire resistance at low and high frequencies and the frequency where $r_w = 2\delta$. Repeat this calculation for the internal inductance. Show that the internal inductance is smaller than the loop inductance, $l_i \ll l$.

3.3 Consider two #28 gauge solid wires ($r_w = 6.3$ mils) separated a distance of 50 mils. Compute the per-unit-length capacitance, c, and inductance, l, by wide-separation approximations and using exact results.

3.4 Repeat Problem 3.3 for one #28 gauge solid wire at a height of 1 cm above a ground plane.

3.5 Determine the per-unit-length capacitance and inductance for the RG-58U coaxial cable which has $r_w = 16$ mils, $r_s = 58$ mils. The interior dielectric is polyethylene with $\varepsilon_r = 2.3$. If the shield has a thickness of 5 mils, determine the per-unit-length resistance of the interior wire and the shield and show that the resistance of the interior wire is the dominant resistance.

3.6 Determine the per-unit-length capacitance and inductance of the three-wire transmission line in Fig. P3.6 on p. 184 by using wide-separation approximations.

3.7 Repeat Problem 3.6 for two wires above ground shown in Fig. P3.7 on p. 184.

3.8 Repeat Problem 3.6 for the coaxial line in Fig. P3.8 on p. 184.

3.9 Prove the relation between the entries in the generalized capacitance matrix, $\mathscr{C}$, and the entries in the transmission-line-capacitance matrix, C, given in (3.19).

3.10 Verify the results given in Tables 3.2 and 3.3.

3.11 Verify the results given in equations (3.105) to (3.109).

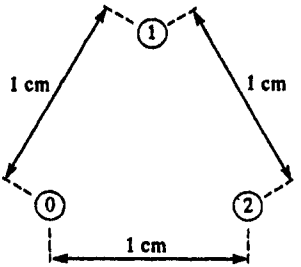

All wires #28 gauge (r_w = 6.3 mils)

FIGURE P3.6

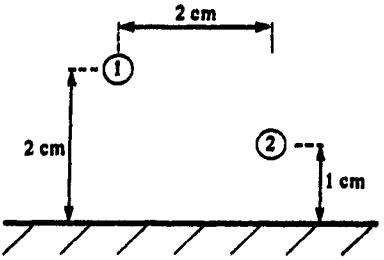

All wires #20 gauge (r_w = 16 mils)

FIGURE P3.7

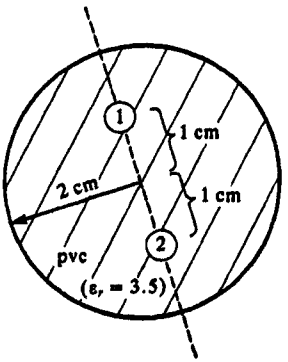

FIGURE P3.8

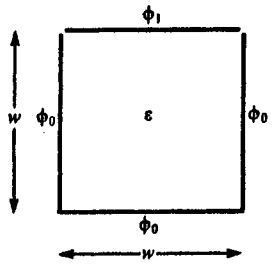

FIGURE P3.12

3.12 A "trough transmission line" is shown in Figure P3.12. Determine the per-unit-length capacitance by using a moment method and the results in (3.105) and (3.107). Confirm your result by a direct solution of Laplace's equation. (See Chapter 10, pp. 588–590 of [A.1].)

3.13 Solve Problem 3.12 by using the finite difference method.

3.14 Solve Problem 3.12 by using the finite element method.

3.15 Determine the per-unit-length parameters with and without dielectric insulations for a three-wire ribbon cable with $d = 50$ mils, $r_w = 18$ mils (#20 gauge), and insulation thickness $t = 7$ mils and $\varepsilon_r = 4$ using the program **RIBBON.FOR**. Plot these for various numbers of expansion coefficients.

3.16 Derive the Galerkin results for equal-width lands given in (3.117).

3.17 Determine the per-unit-length parameters for a PCB consisting of three identical lands with $w = s = 8$ mils and a silicon substrate with 10 mil thickness and $\varepsilon_r = 12$ using the programs **PCB.FOR** and **PCBGAL.FOR**.

3.18 Show that the capacitance matrix is related as in (3.171) to a matrix that is independent of the properties of the surrounding homogeneous medium.

3.19 Investigate the solution of the diffusion equation in cylindrical coordinates given in (3.190).

3.20 Solve the diffusion equation numerically using the finite difference method for a rectangular bar of width w and thickness t.

3.21 Verify the approximate relations for internal impedance of a conductor in the frequency domain given in (3.225).